



Article

Single-cell profile reveals the landscape of cardiac immunity and identifies a cardio-protective Ym-1^{hi} neutrophil in myocardial ischemia–reperfusion injury

Yalan Dong ^{a,b,1}, Zhenyu Kang ^{a,1}, Zili Zhang ^{a,1}, Yongqiang Zhang ^c, Haifeng Zhou ^a, Yanfei Liu ^d, Xinxin Shuai ^e, Junyi Li ^a, Liangqingqing Yin ^a, Xunxun Wang ^a, Yan Ma ^a, Heng Fan ^a, Feng Jiang ^f, Zhihao Lin ^g, Congzhu Ding ^c, Kim Yun Jin ^h, Alexey Sarapultsev ⁱ, Fangfei Li ^j, Ge Zhang ^k, Tian Xie ^e, Changjun Yin ^{l,m,n}, Xiang Cheng ^{b,e}, Shanshan Luo ^{o,*}, Yue Liu ^{d,*}, Desheng Hu ^{a,b,p,*}

^a Department of Integrated Traditional Chinese and Western Medicine, Union Hospital, Tongji Medical College, Huazhong University of Science and Technology, Wuhan 430022, China

^b Hubei Key Laboratory of Biological Targeted Therapy, Union Hospital, Tongji Medical College, Huazhong University of Science and Technology, Wuhan 430022, China

^c Nanjing Drum Tower Hospital, Clinical College of Traditional Chinese and Western Medicine, Nanjing University of Chinese Medicine, Nanjing 210008, China

^d National Clinical Research Center for Chinese Medicine Cardiology, Xiyuan Hospital, Chinese Academy of Chinese Medical Sciences, Beijing 100091, China

^e Department of Cardiology, Union Hospital, Tongji Medical College, Huazhong University of Science and Technology, Wuhan 430022, China

^f Department of International Education, Tianjin University of Traditional Chinese Medicine, Tianjin 300193, China

^g Institute of Neuroscience, School of Medicine, Xiamen University, Xiamen 361102, China

^h School of Traditional Chinese Medicine, Xiamen University Malaysia, Sepang 43900, Malaysia

ⁱ School of Medical Biology, South Ural State University, Chelyabinsk 620049, Russia

^j Shum Yiu Foon Sum Bik Chuen Memorial Centre for Cancer and Inflammation Research (CCIR), School of Chinese Medicine, Hong Kong Baptist University, Hong Kong 999077, China

^k Institute of Integrated Bioinformatic and Translational Science, School of Chinese Medicine, Hong Kong Baptist University, Hong Kong 999077, China

^l Division of Vascular Surgery, The First Affiliated Hospital of Sun Yat-sen University, Guangzhou 510080, China

^m Institute of Precision Medicine, The First Affiliated Hospital of Sun Yat-sen University, Guangzhou 510080, China

ⁿ Institute for Cardiovascular Prevention (IPEK), Ludwig-Maximilians-University, Munich 80336, Germany

^o Institute of Hematology, Union Hospital, Tongji Medical College, Huazhong University of Science and Technology, Wuhan 430022, China

^p China-Russia Medical Research Center for Stress Immunology, Union Hospital, Tongji Medical College, Huazhong University of Science and Technology, Wuhan 430022, China

ARTICLE INFO

Article history:

Received 14 August 2023

Received in revised form 11 December 2023

Accepted 19 January 2024

Available online 7 February 2024

Keywords:

Myocardial ischemia–reperfusion injury

Neutrophil

Ym-1

Cardiac immune response

Single-cell sequencing

ABSTRACT

Myocardial ischemia–reperfusion injury (MIRI) is a major hindrance to the success of cardiac reperfusion therapy. Although increased neutrophil infiltration is a hallmark of MIRI, the subtypes and alterations of neutrophils in this process remain unclear. Here, we performed single-cell sequencing of cardiac CD45⁺ cells isolated from the murine myocardium subjected to MIRI at six-time points. We identified diverse types of infiltrating immune cells and their dynamic changes during MIRI. Cardiac neutrophils showed the most immediate response and largest changes and featured with functionally heterogeneous subpopulations, including Ccl3^{hi} Neu and Ym-1^{hi} Neu, which were increased at 6 h and 1 d after reperfusion, respectively. Ym-1^{hi} Neu selectively expressed genes with protective effects and was, therefore, identified as a novel specific type of cardiac cell in the injured heart. Further analysis indicated that neutrophils and their subtypes orchestrated subsequent immune responses in the cardiac tissues, especially instructing the response of macrophages. The abundance of Ym-1^{hi} Neu was closely correlated with the therapeutic efficacy of MIRI when neutrophils were specifically targeted by anti-Lymphocyte antigen 6 complex locus G6D (Ly6G) or anti-Intercellular cell adhesion molecule-1 (ICAM-1) neutralizing antibodies. In addition, a neutrophil subtype with the same phenotype as Ym-1^{hi} Neu was detected in clinical samples and correlated with prognosis. Ym-1 inhibition exacerbated myocardial injury, whereas Ym-1 supplementation

* Corresponding authors.

E-mail addresses: 2018XH0258@hust.edu.cn (S. Luo), liuyueheart@hotmail.com (Y. Liu), desheng.hu@hust.edu.cn (D. Hu).

¹ These authors contributed equally to this work.

significantly ameliorated injury in MIRI mice, which was attributed to the tilt of Ym-1 on the polarization of macrophages toward the repair phenotype in myocardial tissue. Overall, our findings reveal the anti-inflammatory phenotype of Ym-1^{hi} Neu and highlight its critical role in myocardial protection during the early stages of MIRI.

© 2024 Science China Press. Published by Elsevier B.V. and Science China Press. This is an open access article under the CC BY license (<http://creativecommons.org/licenses/by/4.0/>).

1. Introduction

Myocardial ischemia–reperfusion injury (MIRI) is a prevalent and serious cardiovascular disease characterized by aseptic inflammation of the ischemic myocardium and border zone tissues. Upon hypoxia and the following reoxygenation, the traumatic myocardium elicits an immune response cascade, manifested as the rapid activation of tissue-resident innate immune cells and further recruitment and infiltration of the circulating cells, including neutrophils, macrophages as well as lymphocytes [1]. The cells jointly participate in the pro-inflammatory effects at the early stage of MIRI and subsequent repair and remodeling of myocardium [1]. Immune responses exert crucial roles in the pathogenesis of MIRI, implying that regulating immune responses within a certain time window may be an effective strategy for treating MIRI. As a new method, single-cell RNA sequencing (scRNA-seq) has unique advantages in uncovering specific cell characteristics and functions and has previously been used to investigate the profile of immune cells in acute myocardial infarction (MI) [2–5]. It is worth noting that MIRI fits the clinical situation better, given the widespread application of coronary recanalization surgery, while the description about the essential role of heart-infiltrating immune cells in MIRI is limited.

As the front line of innate immunity, neutrophils can soon be mobilized in response to stimuli, exerting effector functions through phagocytosis, degranulation, and the release of neutrophil extracellular traps [5]. Owing to their short lifespan and inability to proliferate at maturity, as well as technical challenges, research on neutrophils lags behind that of other cell types. Previous studies have mostly focused on macrophages and their high plasticity in mediating injury and repair of the ischemic myocardium. However, recent evidence suggests that neutrophils play a vital role in both mononuclear macrophage recruitment and anti-inflammatory phenotype reprogramming of macrophage [6–8]. Neutrophils are used to be considered as the pro-inflammatory-specific cells, and also the main players of ischemia–reperfusion injury [7]. However, it is worth noting that many attempts on developing anti-neutrophil therapies for MIRI are largely unsuccessful, highlighting the complicated functions of neutrophils [5]. Neutrophils can promote angiogenesis, which is essential for tissue repair [9]. Meanwhile, neutrophils are also reported to undergo a time-dependent polarization process similar to macrophage polarization during MI [10]. In short, pro-inflammatory neutrophils are dominant in the early stage of MI, whereas anti-inflammatory neutrophils are subsequently transformed, highlighting their heterogeneity [10]. However, neutrophil heterogeneity and the exact functions of neutrophil subsets in the process of MIRI are poorly understood, and it remains unclear whether a unique phenotype of neutrophils with unique functions may exist in the heart.

In this study, we use scRNA-seq to analyze the characteristics of infiltrated CD45⁺ cells in the murine heart at six consecutive time points during MIRI, and further comprehensively analyze the cardiac immune status under the pathological conditions. We identify neutrophils as the main population displaying immediate and dramatic changes in the early stages of the cardiac immune response and describe subclusters with different functions according to their unique molecular characteristics. These clusters contribute to

inflammation in the early stages of MIRI and the subsequent repair of myocardial tissue, which is presented not only in the form of cellular heterogeneity but also of time-dependent diversity. Meantime, we also identify a unique population of neutrophils involved in pathological processes of MIRI that exhibit a cardioprotective role and preliminarily determine its potential mechanisms and clinical prospects. These findings provide a foundation for developing new therapeutic strategies involving MIRI-targeting neutrophils.

2. Materials and methods

2.1. Animals

Eight-week-old male C57BL/6J mice were purchased from Beijing Vital River Laboratory Animal Technology Co., Ltd. (Beijing, China). All animal experiments were performed at the animal center of Tongji Medical College, Huazhong University of Science and Technology (HUST), and strictly in accordance with the guidelines of the Animal Research Institute Committee of HUST. The Institutional Animal Care and Use Committee (IACUC) of HUST approved and monitored all procedures (IACUC number: 3554). All applicable institutional and/or national guidelines for the care and use of animals were followed.

2.2. Model construction of myocardial ischemia–reperfusion injury

The MIRI mouse model was established as described previously [11]. Briefly, after adaptive feeding, mice were anesthetized with pentobarbital (70 mg/kg), followed by endotracheal intubation, and a small animal ventilator was connected to maintain breath of the treated mice. After skin preparation, the mice were subjected to a left parasternal incision thoracotomy. Sterile 6–0 silk suture was used to tighten the exposed left anterior descending coronary artery accompanied with PE-10 tubing to facilitate the untying of the knot. After 30 min of ischemia, ligation was released for reperfusion. The skin was sutured, and the mice were kept warm to enable resuscitation from the surgery. The sham operation was performed in the same process except for the coronary artery ligation.

2.3. Cell isolation for single-cell sequencing

CD45⁺ cells were isolated from single-cell suspensions prepared from mouse hearts in the sham or MIRI-induced groups after reperfusion at 0 h, 6 h, 1 d, 3 d and 7 d according to a previous description with minor revisions [2,11]. Briefly, after sacrifice, the mice were immediately perfused through the left ventricle with pre-cooled phosphate-buffered saline (PBS). Then, the hearts were harvested and placed in PBS for further cleaning to completely wash out the blood from the cavities of the heart. After being fully cut into pieces, the heart tissue was digested with 4 mL of HEPE (Gibco, USA, Cat# 15630–080) buffer containing 2 mg/mL Collagenase II (Worthington, USA, Cat# LS004176) combined with DNase I (0.5 mg/mL, Sigma, USA, Cat# 10104159001) at the constant temperature of 37 °C for 30 min with shaking. The RPMI 1640 medium

(Gibco, Cat# C11875500CP) containing 10% fetal bovine serum (Gibco, Cat# 10099141) was used to terminate digestion, and the cell suspension was filtered with a 40-m cell strainer (Corning, USA, Cat# 431750). Incompletely digested tissue was gently ground and washed with 1640 medium for further cell collection. Density gradient centrifugation by lymphocyte separation medium (MP Biomedicals, USA, Cat# 1692249) combined with granulocyte separation solution (Sigma, HISTOPAQUE®-1119) was used to purify infiltrated immune cells from the heart. Then the isolated cells were harvested and incubated with anti-mouse CD45 magnetic microbeads (Miltenyi, Germany) on ice for 15 min followed by two positive selections using a MACS separator (Miltenyi, Cat# 130-042-401). Finally, the CD45⁺ cells infiltrated in the heart were collected. A dead cell removal kit (Miltenyi, Cat# 130-090-101) was used to remove the dead cells according to the manufacturer's protocol. The purity of the isolated cells was detected by flow cytometry, and the activity of the cells was determined by trypan blue staining.

2.4. Library preparation and sequencing

Single-cell RNA sequencing was performed with the purified suspension of myocardial infiltrated CD45⁺ cells with >85% purity and >90% viability (Fig. S1a online). Single cells were captured using the BD Rhapsody system in accordance with the manufacturer's instructions. Briefly, more than 200,000 microwells per chip were randomly deposited in more than 20,000 mixed CD45⁺ cells per chip at two-time points at a ratio of 1:1. Magnetic beads with oligonucleotide barcodes were added to the microwells to pair each bead to a cell. After lysing the cells in the microwells, the magnetic beads were hybridized with polyadenylated RNA molecules, and all beads were retrieved into an Eppendorf tube and washed according to the manufacturer's protocol. Whole-transcriptome libraries were constructed according to the BD Rhapsody single-cell whole-transcriptome amplification workflow. In short, after reverse transcription with the PCR amplifier, a unique molecular identifier and a cell label bar-code were tagged on the 5' end of each cDNA molecule. Next, second-strand cDNA was synthesized, and the WTA adaptor for universal amplification was ligated. An 18-cycle PCR was performed to amplify the adaptor-ligated cDNA. The 3' ends of the transcripts linked with the unique molecular identifier and bar code were enriched with the random priming PCR strategy of the whole-transcriptome amplification products. The quality and quantity of the PCR products were assessed using a High-Sensitivity DNA chip (Agilent, USA) on an Agilent 2200 TapeStation and a Qubit High-Sensitivity DNA assay (Thermo Fisher Scientific, USA), respectively. The final libraries were diluted, multiplexed, and sequenced with a paired-end (75 bp) run on a MGISEQ-2000 by BGI Genomics Co., Ltd (Shenzhen, China).

2.5. scRNA-seq data analysis

After being processed and examined with BD Rhapsody Whole Transcriptome Analysis pipeline, raw sequencing data were presented as a gene expression matrix, which was imported into the Seurat R package for subsequent analysis [12,13]. Fig. S1b (online) shows that almost all cells expressed *Ptprc*, a gene encoding CD45. The cells expressing <100 unique genes were subsequently filtered out, as were those with >25 mitochondria mapping reads. Global mapping statistics, including cell counts, genes per cell, reads per cell, and mitochondria read percentages before and after quality control, are displayed in Fig. S1c and d (online). The FindClusters function was used for cluster analysis, and the clusters were annotated according to the expression of known gene markers. Differentially expressed gene (DEG) analysis of different cells was

performed using FindAllMarkers function and filtered using the following setting (only.pos = TRUE, min.pct = 0.25, logfc.threshold = 0.2). DEGs with an adjusted *P*-value <0.05 (Wilcoxon test) were retained. ClusterProfiler R package was used to perform Gene Ontology (GO) enrichment analysis. The statistical threshold (*q* value Cutoff = 0.05) was applied for the selection of results, and the biological process to which the results belonged was reserved.

2.6. Pseudotime analysis

Pseudotime analysis was constructed using Monocle3 package with default parameters to deduce the potential lineage differentiation trajectories [2]. The DDRTree dimensionality reduction algorithm was used to plot the structure of the trajectory in two-dimensional space.

2.7. Cell-cell communication and signaling pathways

The normalized expression matrix derived from Seurat was input into CellphoneDB, and cell-cell communication analysis was performed [2]. The ligand-receptor pairs featuring an ineffective mean expression, which was calculated as the mean of the average expression of the receptor in one cluster and the ligand in the other, were filtered out. The CellChat package was used for cell-cell signaling pathways analysis.

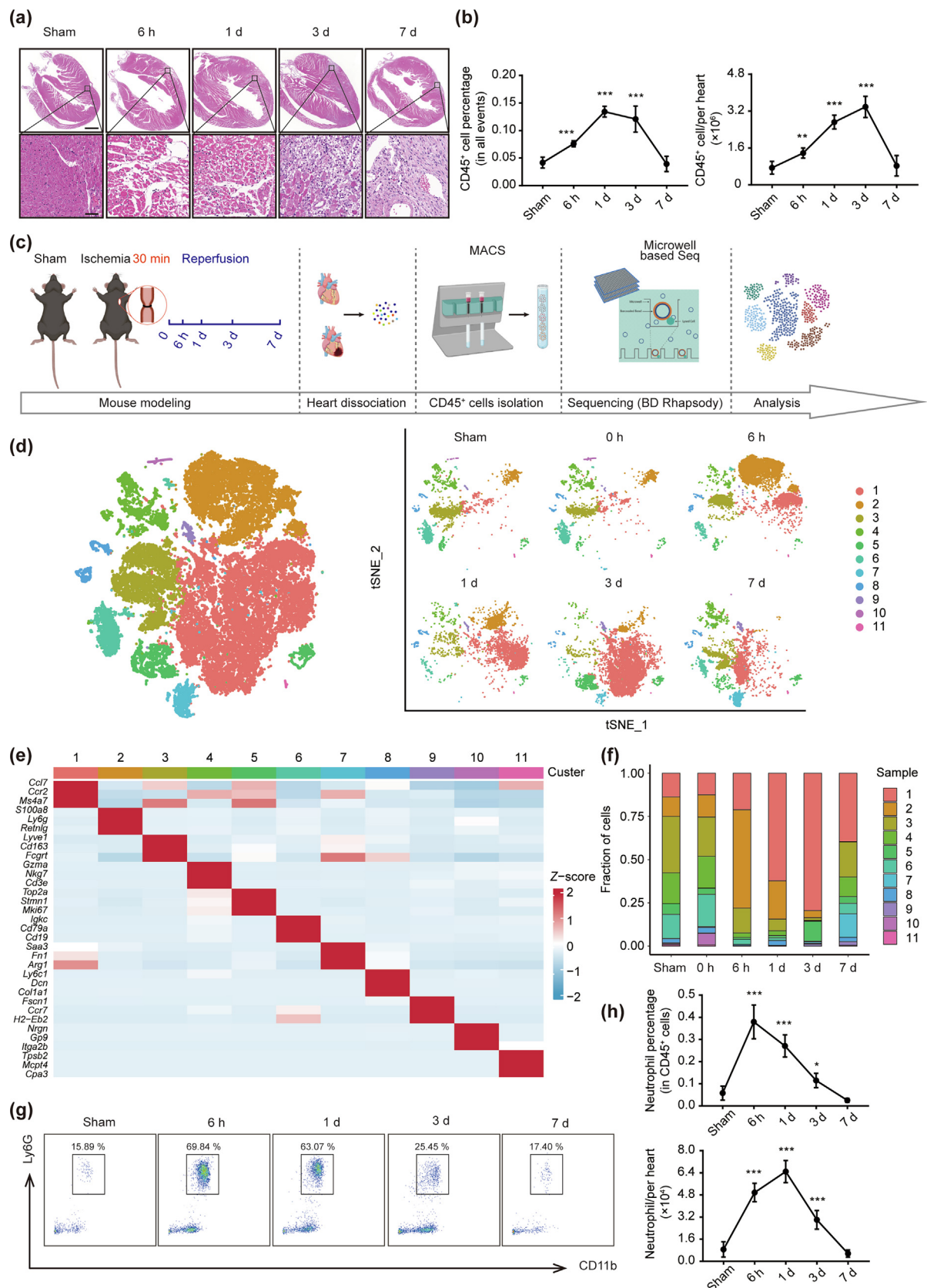
2.8. Histopathological assessment

Whole hearts were isolated and fixed in 4% paraformaldehyde at room temperature (RT) for 24 h. Then, the hearts were embedded in paraffin and sectioned along the long axes at a thickness of 4 μm. All sections were deparaffinized and hydrated using descending concentrations of alcohol prior to staining. Standard hematoxylin and eosin (HE) staining was conducted to evaluate cardiac cell morphology and inflammatory cell infiltration as previously described [11]. After staining, ascending concentrations of alcohol and xylene were used for dehydration; sections were then covered with a coverslip and aired. Histological images of the stained sections were obtained using a panoramic scanner (3DHISTECH Pannoramic MIDI, Hungary) and captured at an appropriate scale using CaseViewer software.

2.9. Immunofluorescence

For tissue immunofluorescence staining, paraffin sections were treated as previously described [11]. In brief, after being deparaffinized and hydrated, the slices were washed with PBS three times and then immersed in the antigen repair solution (Beyotime, China, Cat# P0083) for epitope repair in a microwave oven at 100 °C for 15 min. The slices were then permeabilized with 0.1% Triton-X-100 (Sigma, Cat# 9036-19-5) and blocked with 5% bovine serum albumin (Boster Bio, China, Cat# AR0009) for 60 min at RT. Subsequently, the sections were incubated with primary anti-MPO antibody (ABmart, China, Cat# MK60111), anti-Ym-1 antibody (Abcam, UK, Cat# ab192029), anti-Chi311 antibody (Proteintech, China, Cat# 12036-1-AP), and anti-Ccl3 antibody (Abcam, Cat# ab179638) at 4 °C overnight. After washing with PBS three times, the corresponding secondary antibodies were used for staining at RT for 1 h in the dark. A quenching prevention coverslip containing 4',6-diamidino-2-phenylindole (DAPI, Beyotime, Cat# C1005) was used for nuclear staining and mounting. A panoramic scanner was used to collect fluorescent images, which were subsequently analyzed using ImageJ software.

For cell staining, the cells were first harvested and fixed with 2% paraformaldehyde on ice for 30 min. After being washed and punched, the cells were blocked and stained in the same manner



as the slices. Then, the cells were resuspended in a DAPI-containing solution and smeared to prepare cell slides as the secondary antibody staining finished. Confocal microscopy (Zeiss LSM780, Germany) and flow cytometry (Beckman CytoFLEX, USA) were used for signal detection.

2.10. Echocardiographic examination

Echocardiographic analysis of all mice was performed by two experienced technicians who were blinded to the setting of experimental groups. Twenty-four hours after reperfusion, the mice were anesthetized with 1.0 vol% of isoflurane for echocardiogram examination using a Vevo 2100 high-resolution microimaging system (Visualsonics, Canada). M-mode imaging was used to obtain the two-dimensional echocardiography of the long and short axes of the left ventricle. Cardiac function was evaluated based on the left ventricular ejection fraction (LVEF), left ventricular fractional shortening (LVFS), left ventricular end-diastolic volume (LVEDV), and left ventricular end-systolic volume (LVESV) measured on echocardiography [11,14].

2.11. Single-cell suspension preparation of bone marrow and spleen and peripheral blood mononuclear cell isolation

Single bone marrow-derived cells were obtained by repeatedly flushing the femoral cavity with both ends of the femur cut [15]. Spleen single-cell suspensions were prepared as described previously, whereby the separated spleen was fully cut and ground, red blood cells were lysed, and single cells were harvested after filter [16]. For the isolation of peripheral blood mononuclear cells, blood was directly collected with red blood cell lysis buffer (Beyotime, Cat# C3702) [17]. The cells were then collected and washed with PBS.

2.12. Flow cytometry analysis

For flow cytometry of tissue infiltrating cells, a tissue single-cell suspension was prepared as described above. Cell suspensions were incubated with fluorophore-conjugated antibodies against the following surface markers: mouse CD45-FITC (BD, USA, clone: 104), Ly6C-PE (BD, clone: AL-21), CD19-PE (BD, clone: 6D5), CD19-APC (BD, clone: 6D5), CD11c-PE/Cy7 (BD, clone: HL3), NK1.1-PE/Cy7 (BD, clone: PK136), CD3-APC (BD, clone: 145-2C11), Ly6G-APC-Cy7 (BD, clone: 1A8), CD4-APC-Cy7 (BD, clone: GK1.5), CD8-eFluor450 (eBioscience, USA, clone: 53-6.7), F4/80-BV421 (BD, clone: T45-2342), and CD11b-BV510 (BD, clone: M1/70). Dead cells were eliminated using Fixable Viability Stain510 (BD, Cat# 564406). All surface markers were stained at 4 °C for 30 min in the dark. After washing, the cells were resuspended with FACS buffer and filtered through a 200-mesh cell strainer, followed by flow cytometry using a CytoFLEX machine. CytExpert software (Version 2.4) was used for Flow cytometry analysis; the gating strategy for each cell population is shown in Fig. S2a (online). For immunostaining of immune cells in the

peripheral blood, bone marrow, and spleen, the obtained single cells were stained as described above for tissue-infiltrated cells and detected using flow cytometry.

2.13. Neutrophil depletion and migrate inhibition *in vivo*

Anti-Lymphocyte antigen 6 complex locus G6D (Ly6G) neutralizing antibody (NAb) (BioXcell, USA, Cat# BE0075-1) was used to deplete neutrophils from mice *in vivo* as described previously [17]. In brief, 50 µg of anti-Ly6G NAb was injected into the mice via the tail vein 24 h before model establishment and 0 h after reperfusion. Anti-IgG2a NAb (BioXcell, Cat# BE0089), the isotype control of anti-Ly6G NAb, was administered at the same time, with the same dose and in the same manner as the model mice to exclude the interference of non-specific antibody epitopes. At 24 h after the first administration of neutralizing antibodies, peripheral blood was collected from the mice, and flow cytometry was performed to determine the neutrophil depletion efficiency.

Anti-Intercellular cell adhesion molecule-1 (ICAM-1) NAb (BioXcell, Cat# BE0020-1) was used to inhibit the migration of neutrophils [18]. Similarly, 40 µg of anti-ICAM-1 NAb was injected via the tail vein 2 h before model establishment and 6 h after reperfusion, and anti-IgG2b NAb (BioXcell, Cat# BE0090) was used as the isotype control. After 24 h of reperfusion, we detected the expression of neutrophils in the peripheral blood and heart tissue using flow cytometry to identify the inhibitory effect of NAb on neutrophil migration.

2.14. Ym-1 inhibition and administration *in vivo*

Anti-Ym-1 antibody (Ym-1 antibody, Abcam, Cat# ab93034) dissolved in PBS and recombinant Ym-1 (rYm-1, SinoBiological, China, Cat# 51165-M08H) dissolved in normal saline (NS) were used for Ym-1 neutralization and exogenous supplementation, respectively. Briefly, 10 µg of Ym-1 antibody or 1 µg of rYm-1 was injected into the pericardial cavity at 0 h post-reperfusion in the model mice. Mice in the other model group were treated with the same volume of isotype control (anti-IgG2a for Ym-1 antibody) or NS pericardial injection for interference eradication.

2.15. Enzymatic assays for assessing cardiomyocyte injury

In the validation experiment *in vivo*, peripheral blood from mice after one day of reperfusion was collected to detect the content of cardiomyocyte injury-related enzymes, including creatine kinase MB (CK-MB), α -hydroxybutyric dehydrogenase (α -HBDH), lactic dehydrogenase (LDH), and aspartate aminotransferase (AST), in plasma. Firstly, a fixed volume of peripheral blood from each mouse was collected in an anti-coagulant tube containing heparin sodium and placed at 4 °C for 30 min. The upper plasma was carefully collected after being centrifuged at 3000 r/min for 15 min and used for the subsequent detection of CK-MB, α -HBDH, LDH, and AST with the respective enzymatic assay kit (Nanjing JianCheng, China) according to the manufacturer's instructions.

Fig. 1. Profiling of cardiac CD45⁺ cells from different time points of the MIRI mouse model using scRNA-seq. (a) Representative cardiac histopathologic images with HE staining from the Sham group and different MIRI groups. (upper scale bar = 500 µm, lower scale bar = 50 µm). (b) Statistical analysis of flow cytometry demonstrates changes in cardiac tissue-infiltrating CD45⁺ cells at different time points after reperfusion. The left side shows the percentage of CD45⁺ cells, and the right side shows the absolute count of cardiac CD45⁺ cells. (c) Schematic overview of the experimental procedure for cardiac CD45⁺ cells at different time points after reperfusion using scRNA-seq. (d) t-SNE plot of the distribution of all subtypes at different time points. Cell's colors indicate different subtypes. (e) Heatmap shows three specific marker genes used to identify all cardiac CD45⁺ cells into 11 clusters. (f) Bar graph showing significant variations in the proportion of all clusters at different time points. (g) Representative images of cardiac neutrophils detected using flow cytometry. (h) Statistical analysis of flow cytometry demonstrating changes in cardiac tissue-infiltrating neutrophils at different time points after reperfusion. Upper panel shows the percentage of neutrophils in CD45⁺ cells, and lower panel shows the absolute count of cardiac neutrophils. Data are presented as mean ± standard deviation (SD). *P < 0.05, **P < 0.01, ***P < 0.001 vs. Sham, n = 5 in each group. Each animal experiment was repeated independently at least three times.

2.16. Infarct size measurement

Evans blue (EB) combined with 2,3,5-triphenyltetrazolium chloride (TTC) staining which was performed on day 3 of reperfusion, was used to evaluate infarct size in MIRI mice [19]. Briefly, the mice were treated according to the mouse MIRI modeling method described above to expose the heart, and the left anterior descending coronary artery was ligated at the original ligation site. The postcava was then exposed from enterocoelia. After the mice were sacrificed, 1 mL of 2% EB solution (Sigma, Cat# 314-13-6) was immediately injected through the postcava; at the same time, the ascending aorta was clamped with hemostatic forceps. After staining blue, the heart was isolated and washed with pre-cooled PBS to remove excess dye and blood. Subsequently, the hearts were cut into 1 mm-thick-tissue slices horizontally from the apex of the heart after storage at –20 °C for 1 h to facilitate cutting. Then, the heart tissues were stained with 2% TTC solution (Solarbio, China, Cat# G3005) at 37 °C for 15–20 min. The stained slices were taken out and fixed with 4% paraformaldehyde at RT overnight, and a stereomicroscope (Olympus, Japan) was used to capture images. After staining, blue indicated normal tissue, red indicated the at-risk area, and white indicated the infarcted area. Each region was outlined, and ImageJ software was used to quantify the size of the infarct area.

2.17. Bone marrow-derived macrophage (BMDM) isolation and differentiation induction

Mouse BMDMs were isolated from the femur. First, a single-cell suspension of the bone marrow was obtained according to the aforementioned preparation method. The cells were resuspended with medium containing M-CSF (30 ng/mL, R&D systems, USA, Cat# 416-ML) and inoculated into Petri dishes after filtering with a 70-μm filter (Miltenyi), washing, and centrifugation. After 5–7 d, the BMDMs were harvested for polarization induction. LPS (100 ng/mL, Sigma) was used to induce M1, whereas IL-4 (10 ng/mL, R&D systems, Cat# 404-ML) was used for M2, as previously described.

2.18. Clinical samples

The acquisition of clinical samples was approved by the Ethics Committee of Union Hospital (Tongji Medical College, HUST, UHCT230929), and each patient was informed of the study. Three atherosclerotic plaque slices were obtained from a previous project. Fresh peripheral blood was obtained from patients with acute MI who underwent percutaneous coronary intervention (PCI). Briefly, 2 mL of peripheral blood samples were collected before and one day after surgery in EDTA anti-coagulant tubes, and the plasma was extracted for Chi3l1 (FineTest, China, Cat# EH0093) and brain natriuretic peptide (BNP) (FineTest, Cat# EH2718) detection by ELISA according to the manufacturer's instructions.

2.19. Statistical analysis

GraphPad Prism Software (Version 8.0) was used for data presentation, and SPSS 22.0 software was used for data analysis. All values are represented as the mean ± standard deviation (SD). Statistical analysis was performed with one-way ANOVA followed by Dunnett's test. The paired *t*-test was used to analyze differences between patients before and after treatment. Pearson's correlation coefficient was used to analyze the correlation between two variables. *P* values less than 0.05 were considered as a significant difference.

3. Results

3.1. Myocardial infiltrated immune cells undergo a dynamic alteration in MIRI

During the pathological process of MIRI, the number of infiltrating CD45⁺ immune cells in the reperfusion areas of the heart sharply increased at around day one and reached a peak on day 3, followed by a gradual reduction with progressively increasing myocardial fibrosis (Fig. 1a, b). This pattern of immune infiltration is similar to that in MI, although the time window of the overall immune response in MIRI is advanced [20]. To better understand the characteristics and dynamic changes in myocardial immune responses at different phases of MIRI, the BD platform was used to perform scRNA-seq analysis on CD45⁺ cells harvested from mouse hearts at a steady state (sham), as well as at reperfusion times of 0 h, 6 h, 1 d, 3 d, and 7 d (Fig. 1c). After quality control, we aggregated the data from 36,091 individual cells across all time points into a single dataset, which was subsequently analyzed and presented using the t-distributed stochastic neighbor embedding (t-SNE) dimensionality reduction implemented in the Seurat package. The origin of the individuals from each time point was marked with different colors, which showed that the distribution of cells at reperfusion times of 6 h, 1 d, 3 d and 7 d were significantly different from those at a steady state (Fig. S2b online). Clustering of the scRNA-seq transcripts yielded 11 clusters of immune cells based on classic marker genes, such as *Ccr2*, *Ms4a7*, and *Arg1* for macrophages, *S100a8* and *Ly6g* for neutrophils, *Cd3e* for T cells, and *Cd19* for B cells (Fig. 1d, e, Table 1 and Fig. S2c online). Based on the significant expression of specific markers and representative genes, all individuals were identified as macrophages (clusters 1, 3, 5, 7), neutrophils (cluster 2), T cells (cluster 4), B cells (cluster 6), collagen-related cells (cluster 8), dendritic cells (cluster 9), megakaryocytes (cluster 10), or mast cells (cluster 11) (Fig. 1e, Table 1, Fig. S2c, d and Table S1 online). Among the cells, macrophages were the most abundant cells, followed by neutrophils (Fig. 1d and Fig. S2c online).

To identify the cell composition at each time point, we determined the relative proportion of each cluster along the sampling time points. The composition of the cell populations was dramatically altered at different time points after reperfusion (Fig. 1f), indicating dynamic changes in the infiltrated immune cells during MIRI. At 6 h after reperfusion, neutrophil numbers increased dramatically and reached a peak. Then, at 1 d and 3 d post-reperfusion, the number of neutrophils decreased as time went on, which was validated using flow cytometry (Fig. 1g, h). Macrophages, the original dominant population at a steady state, started to increase at 1 d and stabilized at a relatively high level till 7 d, followed by the up-regulation of T and B cells (Fig. 1f). Notably, at 7 d post-reperfusion, the proportions of different cell types

Table 1
Top differentially expressed genes and cell types of each cluster.

Cluster number	Top differentially expressed genes	Cluster name
1	<i>Ccl7</i> , <i>Ccr2</i> , <i>Ms4a7</i>	Macrophage1
2	<i>S100a8</i> , <i>Ly6g</i> , <i>Retnlg</i>	Neutrophil
3	<i>Lyve1</i> , <i>Cd163</i> , <i>Fcgrt</i>	Macrophage2
4	<i>Gzma</i> , <i>Nkg7</i> , <i>Cd3e</i>	T cell
5	<i>Top2a</i> , <i>Stmn1</i> , <i>Mki67</i>	Macrophage3
6	<i>Igk</i> , <i>Cd79a</i> , <i>Cd19</i>	B cell
7	<i>Saa3</i> , <i>Fn1</i> , <i>Arg1</i>	Macrophage4
8	<i>Ly6c1</i> , <i>Dcn</i> , <i>Col1a1</i>	collagen-related cell
9	<i>Fscn1</i> , <i>Ccr7</i> , <i>H2-Eb2</i>	Dendritic cell
10	<i>Nrgn</i> , <i>Gp9</i> , <i>Itga2b</i>	Megakaryocyte
11	<i>Tpsb2</i> , <i>Mcpt4</i> , <i>Cpa3</i>	Mast cell

largely regressed to that of homeostasis, suggesting self-control of the disease (Fig. 1d, f).

In summary, the results indicate that diverse immune subsets and a dynamic change in myocardial infiltrated immune cells existed during MIRI pathology, which jointly constituted macroscopic cardiac inflammation, with neutrophils being the immediate responders.

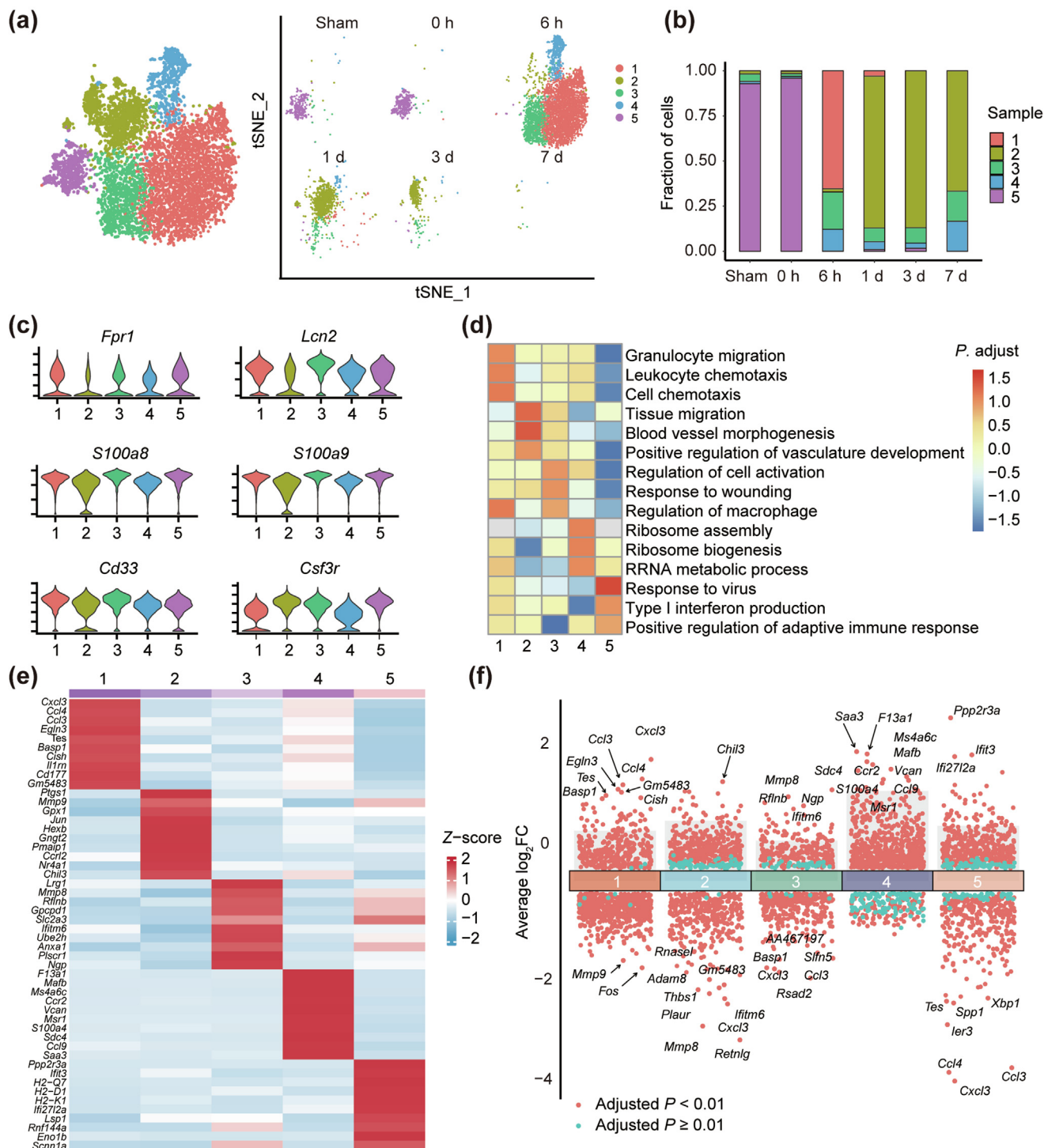
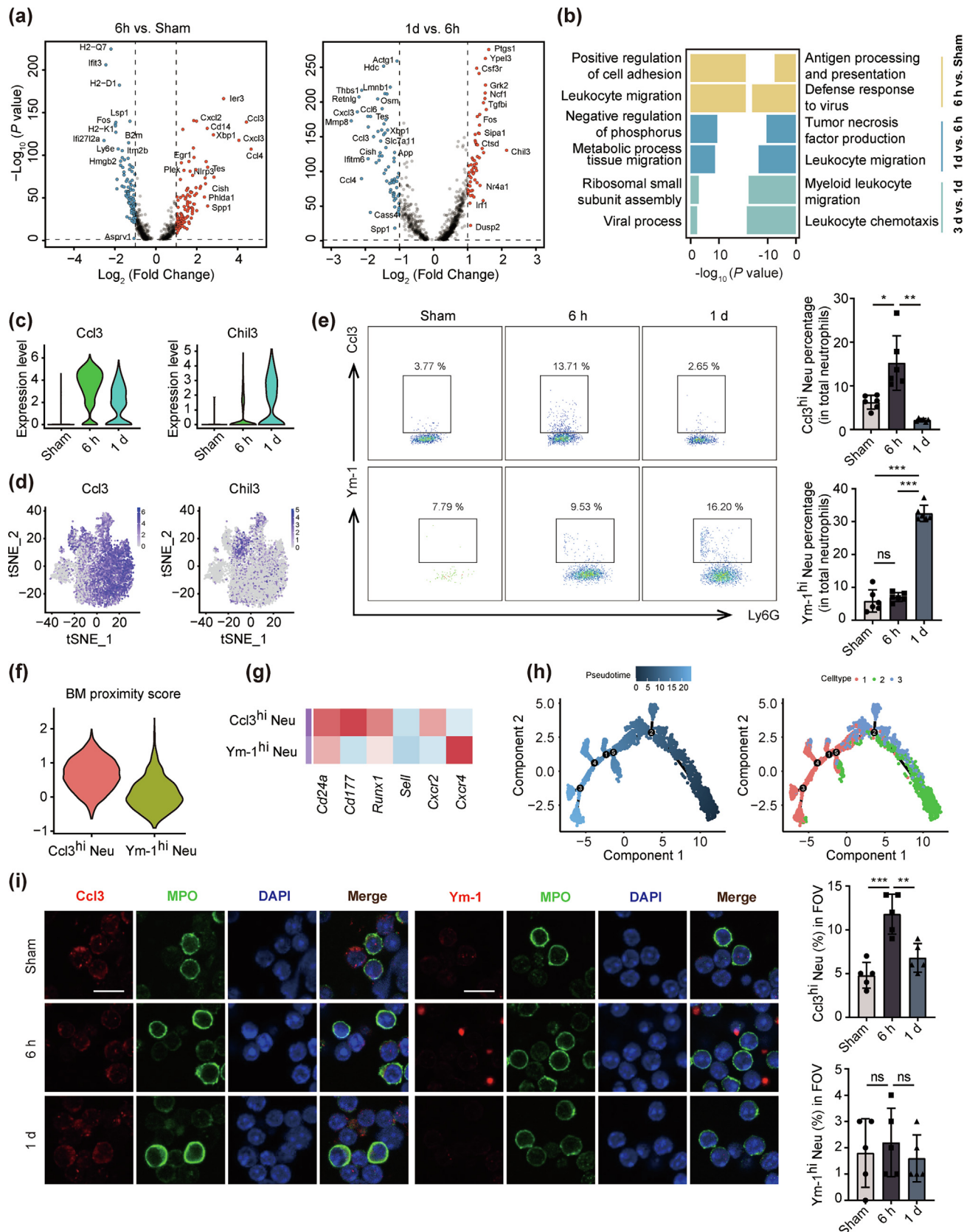


Fig. 2. High heterogeneity and functional difference of cardiac neutrophils during MIRI progression. (a) t-SNE plot of the distribution of all neutrophils at different time points. Cell colors indicate their cluster designation. (b) Bar graph showing variations in the proportion of neutrophil subsets among different time points. (c) Violin plots showing the expression of representative genes of neutrophils (including *Fpr1*, *Lcn2*, *S100a8*, *S100a9*, *Cd33*, *Csf3r*) in each subset. (d) GO analysis showing the specific functional characteristics of five neutrophil subsets. (e) Heatmap of top 10 marker genes used to identify all neutrophils into five clusters. (f) Upregulated and downregulated genes across the five clusters according to differential gene expression analysis. FC indicates fold change; The red dot indicates the adjusted $P < 0.05$; The green dot indicates adjusted $P > 0.05$.



also heterogeneous [5,21], secondary clustering analysis was performed to identify their subpopulation. A total of 7638 neutrophils were extracted from each time point for further analysis, which was confirmed using neutrophil-specific marker genes (*S100a8*, *Cxcr2*, and *Ly6g*) [5] (Fig. S3a online). First, we analyzed the distribution pattern of all neutrophils, and five clusters with unique transcriptional profiles and functions were identified (Fig. 2a and Table S2 online). Next, all neutrophils were colored differently at different time points, with the cells exhibiting a time-dependent appearance (Fig. S3b online). Among them, cells from reperfusion times of 6 h and 1 d accounted for the vast majority of neutrophils (Fig. 2a and Fig. S3b online), indicating rapid recruitment of neutrophils in the early stages of MIRI. As the absolute cell count at each time point was affected by cell separation, the proportion of each cluster was analyzed to identify the neutrophil subsets at each specific time point. The results showed that each neutrophil subset was significantly altered at each time point (Fig. 2a, b). In the steady state, the vast majority of neutrophils was Neutrophil 5 (Neutro5) which was almost absent after MIRI. At 6 h post-reperfusion, Neutro1 was the dominant group, followed by Neutro3 and Neutro4. However, 1 d after reperfusion, Neutro2 expanded rapidly, accompanied by a decrease in Neutro1 compared to that at 6 h post reperfusion. On day 3, the ratio of neutrophil subsets was close to that on day 1 but was characterized by a further decrease in Neutro1. The infiltrated neutrophils at 7 d after reperfusion were Neutro2, Neutro3, and Neutro4. Worth noting is that Neutro3 and Neutro4 were observed at all time points after reperfusion and exhibited relatively stable changes during the pathological process of MIRI.

Next, various clusters of neutrophils, and their functions were characterized according to the expression of unique genes. We examined the expression of conventional neutrophil markers, including *Fpr1*, *Lcn2*, *Cd33*, *S100A8/9*, and *Csf3r* [2,5], and found that all clusters highly expressed representative genes (Fig. 2c). The enriched unique genes of Neutro1, such as *Cxcl3*, *Ccl4*, *Ccl3*, and *Cxcl2* (Fig. 2e and Table S2 online), were closely related to the up-regulation of leukocyte adhesion and migration (Fig. 2d and Fig. S3c online). The high expression of *Basp1*, *Cish*, and *Il1rn* indicates the pro-inflammatory properties, which may be essential factors in the early progression of MIRI. Furthermore, the expression of genes such as *Xbp1* and *Hif1* in Neutro1 was also specifically increased (Table S2 online). Neutro2 expanded rapidly 1 day after reperfusion, with enriched genes contributing to angiogenesis (*Ptg51* and *Mmp-9*) [22] (Fig. 2e and Table S2 online). Further analysis indicated that Neutro2 was enriched in GO terms closely associated with repair functions, including blood vessel morphogenesis and positive regulation of vasculature development (Fig. 2d and Fig. S3c online). Although some highly expressed pro-inflammatory genes, such as *Jun* and *Fos*, were also present in Neutro2 (Table S2 online), the selective expression of genes with myocardial protective effect (*Gpx1*, *Laptm5*, and *Zfp36L2*) [23–25]

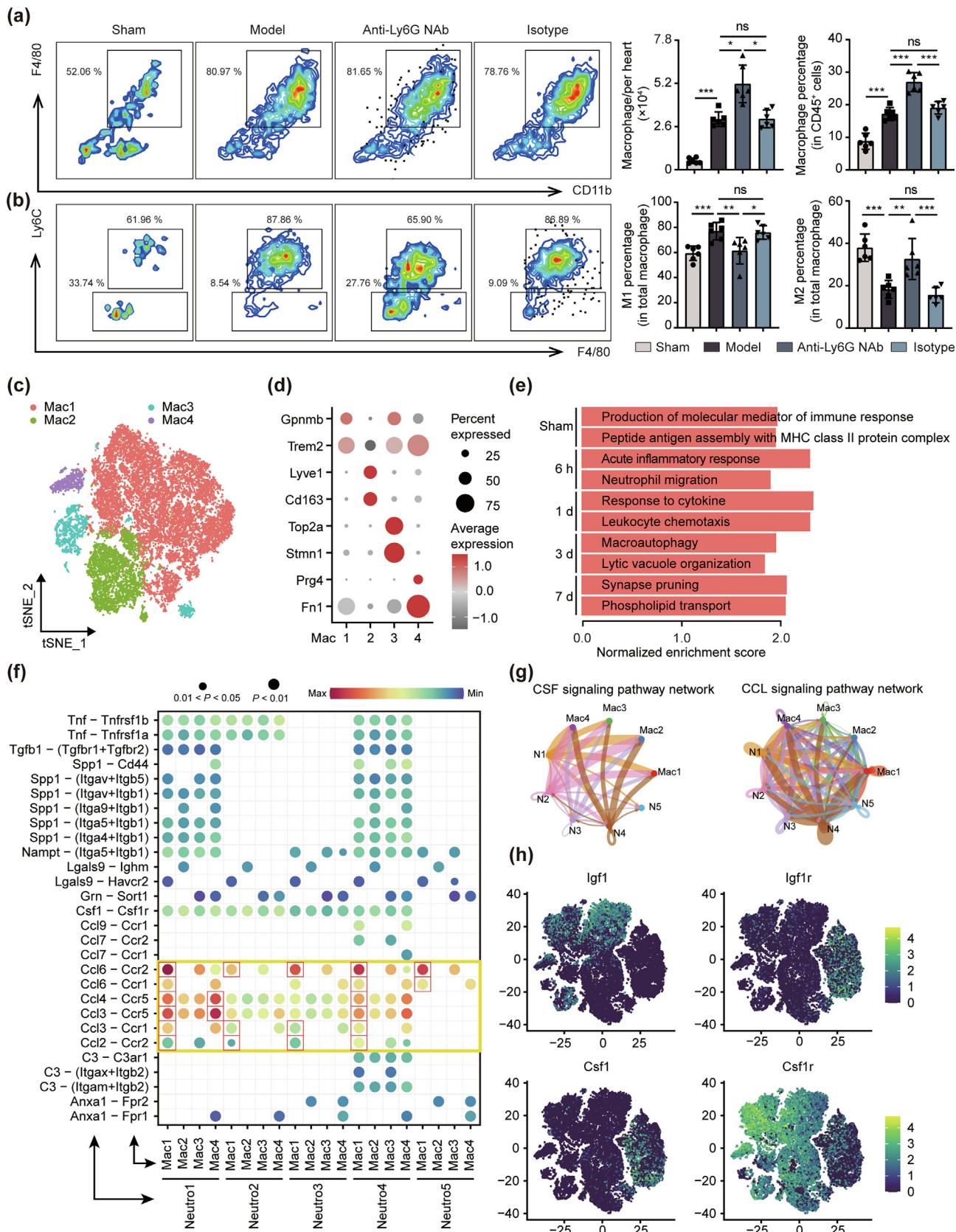
demonstrated the anti-inflammatory potential of Neutro2, which is consistent with the anti-inflammatory neutrophils observed in other studies [5]. Notably, *Chil3*, also known as Ym-1, a unique highly expressed gene in Neutro2, contributes to wound healing [26] (Fig. 2f, Fig. S3d online). Neutro3, which shared genetic features with Neutro1, was closely related to the regulation of cell activation and the response to wounding (Fig. 2d and Fig. S3c online). In addition, differentially expressed pro-inflammatory genes in Neutro3, such as *Mmp-8*, *Lrg1*, *Alox5ap*, *Ifitm2*, and *S100a9*, indicated a somewhat similar function to Neutro1. Moreover, in the low-resolution cluster analysis, Neutro1 and Neutro3 could be grouped into a single cluster (Fig. S3e online). Similar to the phenotype of neutrophil subpopulations in MI in a mouse model [5], Neutro4 was characterized by high expression of transcripts encoding ribosomes (Fig. 2d and Fig. S3c online). Meanwhile, Neutro4 also exhibited an up-regulation of genes that were strongly related to both pro-inflammation and phagocytosis (i.e., *Ms4a6c*, *Mfab*, *Msr1*, *Ms4a8a*) [27] (Fig. 2e, f). *Ccr2* is a hallmark of macrophages migrating from peripheral circulation [2]; thus, the unique high expression of *Ccr2* in Neutro4 indicated that this cluster migrated from the periphery in the early stage of MIRI and belonged to a post-infarction inflammatory cluster (Fig. 2e, f). Neutro5 expressed signature genes of MHC-II (*H2-Q7*, *H2-D1*, and *H2-K1*), thereby exhibiting an antigen-presenting phenotype (Fig. 2e). In addition, Neutro5 were enriched with antiviral-related genes responsible for type I interferon production (Fig. 2d and Fig. S3c online), indicating its role in pro-inflammatory response. Notably, Neutro5 accounted for the vast majority of neutrophils at homeostasis with the conventional identified function (Fig. 2b, d). Given that a few tissue-infiltrating neutrophils exist in homeostasis, Neutro5 may also represent resident neutrophils in cardiac microvessels.

In summary, during the pathogenesis of MIRI, cardiac neutrophils underwent dynamic changes and comprised three pro-inflammation subsets: Neutro1, Neutro3, and Neutro4; anti-inflammation Neutro2; and APC-like Neutro5. According to the dominant expression patterns and uniquely expressed genes of *Ccl3* and *Chil3* (Fig. S3d online), Neutro1 and Neutro2 are referred to as *Ccl3^{hi}* Neutrophils (*Ccl3^{hi}* Neu) and *Ym-1^{hi}* Neutrophils (*Ym-1^{hi}* Neu), respectively.

3.3. Anti-inflammatory *Ym-1^{hi}* Neu is specifically expressed in infarcted hearts

According to previous studies and our data, neutrophils are mainly involved in the early stages of the pathological process of reperfusion injury [5,7]. Thus, we mainly focused on the characteristics of neutrophils at reperfusion times of 6 h and 1 d after MIRI. DEGs and enriched biological processes derived from GO analysis for the indicated time point were analyzed to elucidate changes in the time-specific molecules in myocardial neutrophils. The

Fig. 3. Time-specific expression and source of predominant cardiac Neutrophil subsets during MIRI progression. (a) Volcano plot of the fold-change in differential gene expression in 6 h MIRI and Sham groups (left) and 1 d MIRI and 6 h MIRI groups (right) from all neutrophil cells. Wilcoxon rank sum test and Bonferroni analysis were used to calculate *P* values for *P* adjusted values, respectively. (b) Critical GO enrichment terms of DEGs in 6 h MIRI and Sham, 1 d MIRI and 6 h MIRI, and 3 d MIRI and 1 d MIRI groups. Upregulated DEGs were enriched in the left-side terms, whereas downregulated DEGs were enriched in the right-side terms. (c) Violin plot of time-specific signature gene expression at different time point. (d) Time-specific gene expression patterns projected onto t-SNE plots. (e) Representative images and statistical analysis of cardiac *Ccl3^{hi}* neutrophils (upper) and *Ym-1^{hi}* neutrophils (lower) at different time points detected using flow cytometry (*n* = 6 in each group). (f) Violin plot showing the BM score of *Ccl3^{hi}* neutrophils and *Ym-1^{hi}* neutrophils. N1 represents *Ccl3^{hi}* neutrophils, and N2 represents *Ym-1^{hi}* neutrophils. (g) Heatmap showing the relative expression of cell senescence associated genes in N1 and N2. (h) Trajectory analysis showing the evolutionary direction of all subpopulations of neutrophils; the evolutionary direction is from right to left. (i) Representative images and statistical analysis of immunofluorescence of N1 and N2 in single splenic cells at different time points (scale bar = 10 μ m, *n* = 5 in each group). Data are presented as the mean \pm SD. **P* < 0.05, ***P* < 0.01, ****P* < 0.001, ns means not significant. Each animal experiment was repeated independently at least three times.



characteristic genes of *Ccl3^{hi}* Neu (i.e., *Ccl4*, *Ccl3*, and *Cxcl3*) were significantly increased at 6 h post-reperfusion, whereas *Chil3* and *Mmp-9*, unique highly expressed genes for *Ym-1^{hi}* Neu, were significantly increased at 1 d after reperfusion (Fig. 3a and Table S3 online). This time-dependent gene expression pattern may be attributed to the predominance of *Ccl3^{hi}* Neu and *Ym-1^{hi}* Neu at specific times. Simultaneously, the expression of some pro-inflammatory cytokines also increased, as evidenced by elevated *Il1rn* and *Il18rap* (Table S3 online). These chemokines and cytokines contributed to the recruitment of inflammatory cells under various stress conditions, as confirmed by GO analysis, whereas the gene-enriched terms of tissue migrating specific to 1 d after reperfusion indicated the tissue repair ability of neutrophils (Fig. 3b and Fig. S4a online). Three days after reperfusion, limited DEGs were mainly enriched in viral defense (Fig. 3b and Fig. S4a online). In addition, *Ccl3* and *Chil3* were well represented as time-specific molecules at 6 h and 1 d of reperfusion, as shown by the violin plot and t-SNE plot, respectively (Fig. 3c, d), indicating the time-specific expression pattern of these two clusters. And uniquely high expression of *Ccl3^{hi}* Neu at 6 h and *Ym-1^{hi}* Neu at 1 d was further confirmed using flow cytometry and immunofluorescence (Fig. 3e and Fig. S4b, c online).

To understand why *Ccl3^{hi}* Neu and *Ym-1^{hi}* Neu exhibit different phenotypes during the progression of MIRI, we further analyzed the characteristics of the upstream cells and their sources. Because of the short lifespan and quick mobilization of neutrophils from the bone marrow (BM) to the injury site [21], we detected neutrophils and granulocyte progenitor cells (GPCs) in the BM, spleen and peripheral blood of mice at 6 h, 1 d, 3 d after reperfusion, as well as in the sham group, using flow cytometry (Fig. S4d online). These data indicated that in the early stages of reperfusion, mature neutrophils were released directly from the BM and circulated to damaged cardiac tissue through the blood and spleen, as evidenced by a gradual increase of GPCs in the BM and a dramatic decrease of neutrophils in the blood (Fig. S4e online). The subsequent increase of GPCs in the BM might also be attributed to the supply of cardiac macrophages in later stages, given that GPCs are common progenitors for neutrophils and macrophages [28]. Thus, tissue-infiltrating neutrophils are more similar to BM-derived neutrophils in the early stages of reperfusion and then gradually acquire an aging phenotype over time. The BM proximity score analysis confirmed that *Ccl3^{hi}* Neu had a higher score than *Ym-1^{hi}* Neu (Fig. 3f), which is consistent with the time-specific variation characterized by a sharp decline in the dominant infiltrated *Ccl3^{hi}* Neu and subsequent rapid expansion of *Ym-1^{hi}* Neu in the early phase of reperfusion. Similarly, *Ccl3^{hi}* Neu over-expressed “young” neutrophil markers (*Cd177/Cxcr2*), whereas *Ym-1^{hi}* Neu showed increased expression of the aging/activation-related gene *Cxcr4*, which was further confirmed by the aging score [2,5] (Fig. 3g and Fig. S4f online).

We then performed pseudotime analysis to elucidate the dynamics and transitions among neutrophil subpopulations over time. The evolution of neutrophils moved from right to left, and

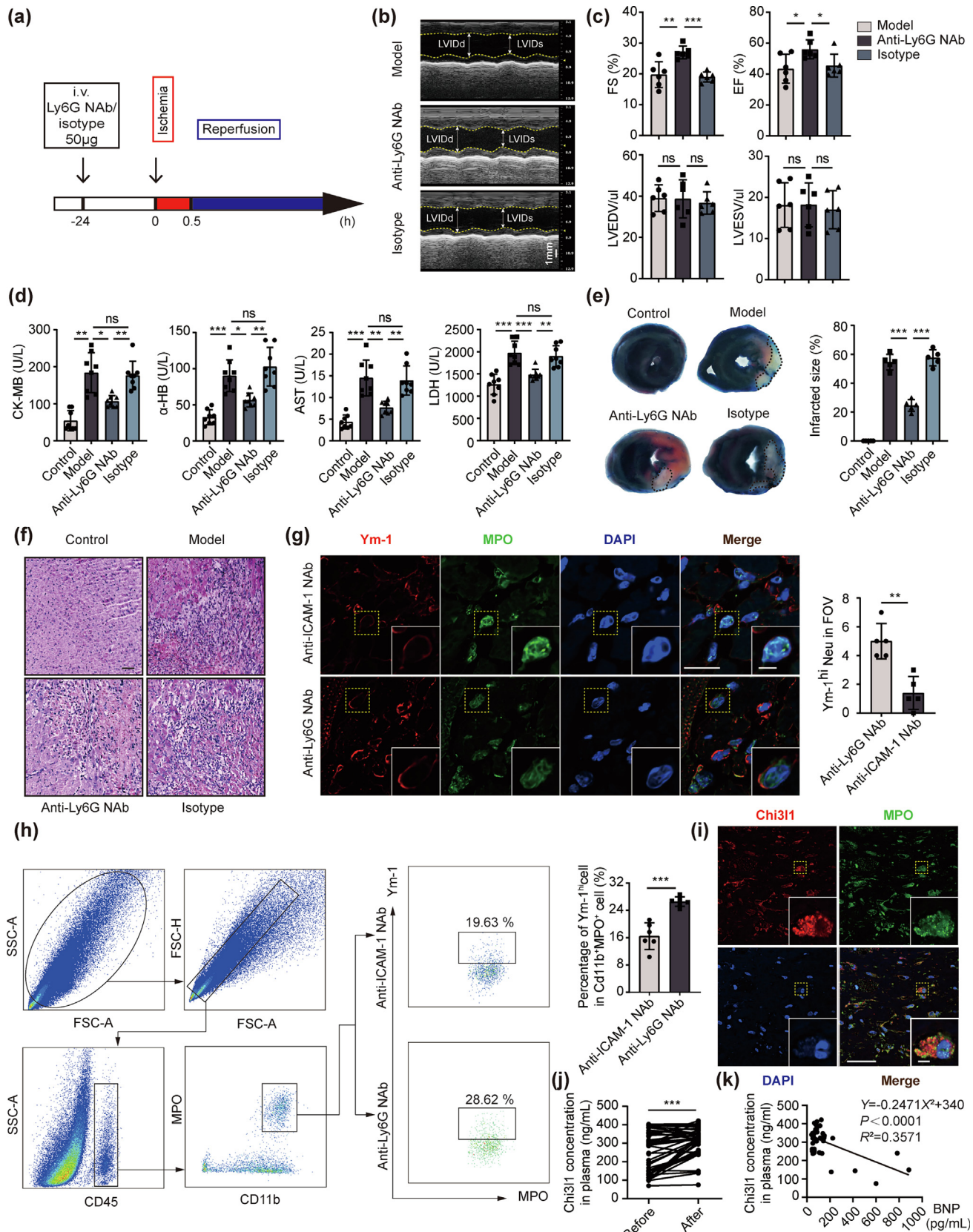
Ccl3^{hi} Neu (cluster 1) and *Ym-1^{hi}* Neu (cluster 2) showed opposite evolutionary directions (Fig. 3h), which agrees with the difference in BM proximity score and changes in the composition ratio over time since reperfusion occurred. As the BM is a repository for immune cells, including neutrophils, before being released to the peripheral [28], we further detected the abundance of *Ccl3^{hi}* Neu and *Ym-1^{hi}* Neu in the BM and spleen at 6 h and 1 d post-reperfusion. Immunofluorescence and flow cytometry analysis indicated that *Ccl3^{hi}* Neu were increased at 6 h after reperfusion in both the BM and spleen, whereas no significant difference in *Ym-1^{hi}* Neu was observed in the periphery at the different time points (Fig. 3i and Fig. S4g, h online). This result, combined with their dynamic expression patterns in the heart, suggests that *Ccl3^{hi}* Neu are BM-mobilizing cells, whereas the phenotype of *Ym-1^{hi}* Neu might be tissue-specific.

3.4. Neutrophils are the pivot of cardiac immune response in the pathological process of MIRI

Owing to the sentinel effect of neutrophils in the pathological process of MIRI, we speculated that the recruitment and activation of neutrophils might be a crucial step in mediating immune cell infiltration in the later stage. Therefore, the CellPhone algorithm was used to analyze the interaction between neutrophils and other immune cells. The data showed that neutrophils interacted not only with macrophages but also with T and B cells of adaptive immunity in the later period of reperfusion (Fig. S5a online). Previous studies have indicated that neutrophils may exert cardioprotective effects by inducing macrophage polarization toward an anti-inflammatory phenotype [8], implying a close relationship between neutrophils and macrophages in the immune activation cascade. As expected, the association between neutrophils and macrophages was the strongest in the interactions between neutrophils and other immune cells in MIRI (Fig. S5a online). To further verify the regulation of neutrophils on macrophages during the pathological process of MIRI, anti-Ly6G neutralizing antibody (NAb) was used to deplete circulating neutrophils in mice. The infiltrated immune cells in the injured cardiac tissue at 3 d after reperfusion were detected using flow cytometry, and the total macrophages were indeed significantly increased with the administration of NAb (Fig. 4a). Consistent with other studies, the administration of anti-Ly6G NAb inhibited the expression of M1 macrophages but promoted the expression of M2 macrophages (Fig. 4b).

ScRNA-seq analysis demonstrated that macrophages were the dominant cluster in both the pathological processes of MIRI and homeostasis (Fig. 1c). To further analyze the interaction between neutrophils and macrophages, we extracted macrophage data (comprising four clusters identified in Fig. 1e) based on the specific expression of cell markers (Fig. 4c, d, Table 1, and Table S1 online). Under homeostasis, the main myocardial subpopulation of macrophages was the tissue-resident macrophages that function in antigen presentation. After reperfusion, inflammatory-related

Fig. 4. Interaction between neutrophils and macrophages during MIRI progression. (a, b) Representative images and statistical analysis of cardiac macrophages ($CD45^+Lin^-CD11b^+F4/80^+$) (a), M1 macrophages ($CD45^+Lin^-CD11b^+F4/80^+Ly6C^+$), and M2 macrophages ($CD45^+Lin^-CD11b^+F4/80^+Ly6C^{low}$) (b) in different groups of mice used to identify the effect of neutrophil depletion by Ly6G NAb on the expression of cardiac macrophages and subsets ($n = 6$ in each group). (c) t-SNE plot of the distribution of all monocyte/macrophages. Cell colors indicate different subtypes. (d) Dot plot of the expression of specific marker genes used to identify monocyte/macrophage subtypes. Dot size indicates the percentage of the cell expressing the marker gene in each cluster. (e) GO analysis showing the time-specific function of all monocytes/macrophages during the progression of MIRI. (f) Dot plot indicating selected ligand-receptor interactions between neutrophils and monocytes/macrophages. Dot size indicates P-values, and color indicates the mean expression level of the paired interacting molecules. (g) Circle plot of the inferred CSF signaling networks (left) and CCL signaling networks (right) among neutrophils and monocytes/macrophages. Line thickness indicates the intensity of the signaling pathway expression. (h) Selected paired ligand-receptor expression pattern projected onto t-SNE plots (upper is *Igf1-Igf1r*, lower is *Csf1-Csf1r*). Data are presented as the mean \pm SD. * $P < 0.05$, ** $P < 0.01$, *** $P < 0.001$, ns means not significant. Each animal experiment was repeated independently at least three times.



macrophages gradually dominated, as evidenced by GO terms associated with the acute inflammation response and inflammatory cell chemotaxis (Figs. 1e and 4e). During the repair phase, macrophages exhibited features of tissue repair, such as macroautophagy and phospholipid transport (Fig. 4e), which is consistent with macrophages being an important cluster mediating damage and repair in MIRI [6]. However, the mechanism by which neutrophils regulate the stage-specific functions of macrophages remains unclear. Therefore, potential communication between neutrophils and macrophages was further investigated, and close associations were found among the subpopulations of the two cells, mainly in the subsets of Neutro1 and Mac1 (Fig. S5c, d online). Next, receptor/ligand analysis was performed to identify the direct connection between neutrophil and macrophage subpopulations. Neutrophil and macrophage subsets were identified as sender (expressing ligands) and recipient cells, respectively. This finding revealed that the CCL signaling pathway, followed by the SPP1 signaling pathway, was the dominant pathway involved in communication between these two cell types (Fig. 4f, g). *Ccl3^{hi}* Neu, which is closely linked to various macrophage subsets, was not only regarded as a sender cell but also as a recipient cell (Fig. 4f), which demonstrated that *Ccl3^{hi}* Neu, recruited by tissue-resident macrophages after reperfusion, further mediated the recruitment of inflammatory macrophages in the early stage of MIRI over time. Furthermore, some ligand-receptor pairs that have been experimentally validated, including *Csf1-Csf1r* and *Igf1-Igf1r* between neutrophils and macrophages [29,30], were relatively highly expressed as receptors or ligands, respectively (Fig. 4h).

In general, in the pathology of MIRI, the recruitment and activation of neutrophils is a key link in the regulation of myocardial immune responses, which affects the subsequent recruitment and function of other immune cells, especially macrophages. Therefore, neutrophil modulation may be an effective strategy for the development of protective reagents against MIRI.

3.5. Increased *Ym-1^{hi}* Neu might exert the cardio-protective effect in MIRI

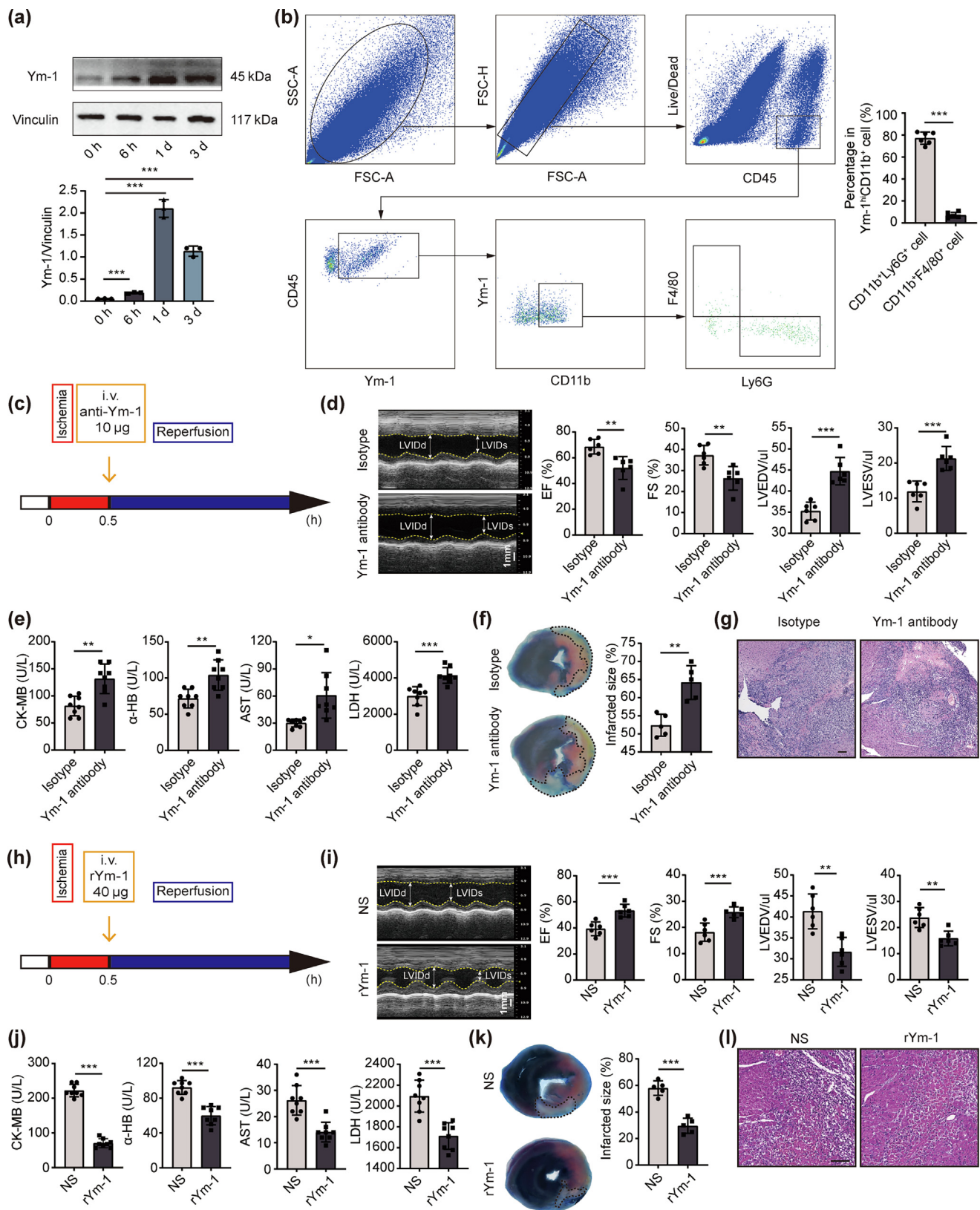
To further clarify the exact effect of targeting neutrophils in MIRI, we performed a series of experiments to deplete or inhibit neutrophil infiltration in the cardiac tissue of MIRI mice. Experimentally, anti-Ly6G NAb was used to deplete neutrophils as mentioned above, with isotype IgG2b as a control (Fig. 5a). Previous studies have shown that anti-Ly6G NAb protects mice against myocardial infarction-induced heart injury [5]. In our study, at 1 d after reperfusion, anti-Ly6G NAb administration significantly improved the cardiac function of MIRI mice, as evidenced by higher LVEF and LVFS than in model mice measured using echocardiography (Fig. 5b, c). While no significant difference was observed in

LVESV or LVEDV among all groups, which might be attributed to the absence of ventricular remodeling in the early stage of reperfusion (Fig. 5c). We also found that the levels of plasma enzymes, including CK-MB, α -HBDH, LDH and AST, were significantly increased in MIRI model mice, whereas anti-Ly6G NAb reversed the upregulation, and no significant difference was observed in the isotype group (Fig. 5d). EB and TTC staining showed that the myocardial infarct size was significantly limited by anti-Ly6G NAb treatment compared to that in the model group, as shown by the smaller white area and a lower ratio of infarct size/left ventricular (Fig. 5e). These data indicate that anti-Ly6G NAb ameliorated cardiac injury in MIRI. Meanwhile, compared with the model and isotype-treated mice, HE staining showed fewer cardiac inflammatory cells and more normal morphology with anti-Ly6G NAb administration at 3 d after reperfusion (Fig. 5f). These results indicate that the partial consumption of neutrophils at the early stage of MIRI contributes to the cardioprotective effect. Next, we treated the model mice with an anti-ICAM-1 NAb, which inhibits neutrophil migration [18]. Anti-ICAM-1 NAb was administrated 2 h before modeling and 6 h after reperfusion, with IgG2b as an isotype control (Fig. S6a online). Cardiac neutrophils were clearly decreased at 1 d after reperfusion in NAb-treated mice but not in the isotype control (Fig. S6b online). We then evaluated the cardio-protective role of anti-ICAM-1 NAb on MIRI according to cardiac function, plasma enzyme levels, infarct size, and histopathological changes, as described above. No significant improvement in cardiac injury was observed with anti-ICAM-1 NAb administration (Fig. S6c–f online), indicating that inhibiting the migration of neutrophils to myocardial tissue did not protect mice from heart injury in the early stage of MIRI.

As both anti-Ly6G and anti-ICAM-1 NAb partially reduced myocardial infiltrated neutrophils in MIRI, we clarified the mechanism behind the efficacy difference between the two individual interventions by further analyzing the phenotypes of myocardial infiltrated neutrophils from mice treated with the two NAb. Given the anti-inflammatory potential and time-specific expression of *Ym-1^{hi}* Neu, we detected the abundance of *Ym-1^{hi}* Neu at 1 d after reperfusion. Although cardiac neutrophils were both decreased by treatment with NAb, the relative amount of *Ym-1^{hi}* Neu in anti-Ly6G NAb treated mice was clearly higher than that in anti-ICAM-1 NAb-treated mice (Fig. 5g, h), suggesting that the abundance of *Ym-1^{hi}* Neu might be the main factor determining the distinct outcomes of the two interventions in MIRI model mice and that *Ym-1^{hi}* Neu might be a crucial cluster mediating the prognosis of MIRI.

Next, we detected the expression of chitinase-3-like protein 1 (Chi3l1), corresponding to *Ym-1*, in clinical samples of atherosclerosis to determine the presence or absence of *Chi3l1^{hi}* Neu in humans. Immunofluorescence showed that abundant neutrophils infiltrated the plaques, some of which were characterized by high

Fig. 5. *Ym-1^{hi}* Neu is involved in the improvement and prognosis of heart injury. (a) Schematic diagram of experimental design. (b) Representative echocardiography of mice in each group 1 d after reperfusion. (LVIDd, left ventricular internal diameter at end-diastole; LVIDs, left ventricular internal diameter at end-systolic.) (c) Statistical analysis of the cardiac function evaluated using the left ventricular ejection fraction (EF), left ventricular fractional shortening (FS), left ventricular end-diastolic volume (LVEDV), and left ventricular end-systolic volume (LVESV). Increased EF and FS and decreased LVEDV and LVESV indicate improved cardiac function ($n = 6$ in each group). (d) Statistical analysis of serum enzymology, including CK-MB, α -HBDH, AST, and LDH, in mice from each group at 1 d after reperfusion ($n = 8$ in each group). (e) Representative Evans blue/TTC staining images of the heart and quantitative analysis of infarct size per cross-section of the left ventricle. The white area indicates infarct tissue, and the red area indicates danger tissue ($n = 5$ in each group). (f) Representative cardiac histopathologic images with HE staining in each group (scale bar = 50 μ m). (g) Immunofluorescence and quantitative analysis of *Ym-1^{hi}* Neu expression 1 d after reperfusion in mice cardiac tissue with the administration of anti-ICAM-1 NAb and anti-Ly6G NAb (left scale bar = 10 μ m, right scale bar = 1 μ m, $n = 5$ in each group). (h) Flow cytometry and quantitative analysis showing the difference in cardiac *Ym-1^{hi}* Neu expression 1 d after reperfusion with the administration of anti-ICAM-1 NAb and anti-Ly6G NAb ($n = 6$ in each group). (i) Immunofluorescence analysis of *Chi3l1^{hi}* Neu expression in human atherosclerotic plaque (left scale bar = 50 μ m, right scale bar = 4 μ m, $n = 3$). (j) Plasma levels of *Chi3l1* from patients with MI receiving PCI at different time points detected using ELISA. “Before” indicates before PCI, and “after” means 1 d after PCI ($n = 40$). (k) Correlation analysis of *Chi3l1* and BNP of patients ($n = 40$). Data are presented as the mean \pm SD. * $P < 0.05$, ** $P < 0.01$, *** $P < 0.001$, ns means not significant. Each animal experiment was repeated independently at least three times.



Chi3l1 expression (Fig. 5i). Given that Ym-1 and Chi3l1 are secreted proteins [31], we detected plasma Chi3l1 levels in patients with MI before and 1 d after PCI to clinically explore the expression profile of Chi3l1. In some patients, we found higher Chi3l1 at 1 d after reperfusion than before surgery (Fig. 5j). Furthermore, correlation analysis between Chi3l1 and BNP, a heart failure indicator, was performed to identify the role of Chi3l1 as a clinical prognostic indicator (Fig. 5k). The results showed that the level of Chi3l1 was significantly negatively correlated with BNP levels, suggesting that Chi3l1 is a protective factor against MIRI in humans.

3.6. Ym-1 in neutrophils contributes to MIRI protection by promoting M2 polarization

To further confirm the cardioprotective role and demonstrate the potential mechanism of action of Ym-1^{hi} Neu in MIRI, we performed inhibition and supplementation of Ym-1 *in vivo*. Given that Ym-1 is a marker for M2 macrophage activation [32], we first identified the expression profile of Ym-1 in cardiac immune cells. Ym-1 was highly expressed 1 d after reperfusion (Fig. 6a) and mostly originated from neutrophils rather than macrophages (Fig. 6b). Therefore, Ym-1 inhibition 1 d after reperfusion was regarded as a functional suppression of Ym-1^{hi} Neu. The Ym-1 antibody was administered since reperfusion occurred with the isotype of IgG2a as a control (Fig. 6c). Cardiac Ym-1 expression was downregulated at 1 d after administration of the antibody (Fig. S7a, b online). Next, we analyzed the degree of heart injury as described above. Notably, worsening cardiac function, increased enzyme levels, a larger infarct size, and an enhanced area of cell infiltration were observed with Ym-1 antibody administration (Fig. 6d–g).

Recombinant Ym-1 was used as an exogenous supplement to investigate its role in the MIRI mouse model (Fig. 6h). Mice that received rYm-1 via pericardial injection after reperfusion exhibited better cardiac function, lower plasma enzyme levels, smaller infarct size, and more normal histomorphology than mice in the model group (Fig. 6i–l), which jointly indicated that Ym-1 exerted a protective effect on MIRI. Notably, a cardioprotective effect was observed following the supplementation of Ym-1 in anti-ICAM-1 NAb-treated mice, compared with the mice that received only anti-ICAM-1 NAb, as measured by cardiac function, plasma enzymology, infarct size, and histopathology (Fig. S8a–e online). However, the mechanism by which Ym-1 affects the pathological process of reperfusion injury remains unclear. Because of the close association between neutrophils and macrophages, as well as the overexpression of M2 macrophages in anti-Ly6G NAb-treated mice, we examined the phenotype of cardiac macrophages in mice administered different treatments at 3 d after reperfusion. The number of infiltrated M2 macrophages was significantly decreased when Ym-1 was inhibited but increased with Ym-1 administration

(Fig. 7a–c), indicating that Ym-1 might contribute to macrophage polarization in the cardiac tissue of MIRI. To further confirm the role of Ym-1 in macrophage polarization, Ym-1 was added to the BMDM cultured *in vitro* with the stimulation of LPS or IL-4. We found that Ym-1 supplementation significantly promoted M2 polarization and simultaneously suppressed M1, as shown by flow cytometry, which was further confirmed by increased Arg-1 and decreased iNOS expression detected using western blotting (Fig. 7d, e). Taken together, these data suggested that Ym-1^{hi} Neu exerts the anti-MIRI effects by promoting macrophage polarization to an anti-inflammatory phenotype.

4. Discussion and conclusion

Owing to the rapid development of MI therapy, MIRI has become a problem that cannot be ignored. MIRI and MI share certain similarities and differences in their pathogenesis [20]. Although many studies have analyzed scRNA-seq data to uncover the dynamic changes in cardiac immune cells in MI, the characteristics of immune cells in MIRI remain unclear. Owing to pathological differences, the time window for immune cell responses in MIRI is significantly earlier than that in MI [20]. Therefore, a comprehensive study of the heterogeneity, origin, and function of cardiac immune cells in MIRI will enhance our understanding of inflammatory responses involved in the pathogenesis of MIRI, thereby providing a fundamental basis for developing effective therapeutic approaches. In this study, we investigated the features of CD45⁺ cells infiltrated in the cardiac tissue of MIRI mice over a long term using scRNA sequencing and further investigated the heterogeneity of neutrophil subsets. Furthermore, based on the characteristics of various neutrophil clusters, we identified a specific Ym-1^{hi} Neu with a cardioprotective effect, which may serve as a target for early intervention in MIRI, as well as their secreted proteins.

Neutrophils play an important role in the pathogenesis of infectious diseases, removing bacteria and dead cells via phagocytosis and promoting wound repair [21]. Neutrophils are key promoters of aseptic inflammation in the heart and also contribute to cardiac repair after MI [5,7,8]. Under the stimulation of ischemia and hypoxia, neutrophils produce reactive oxygen species, neutrophil extracellular traps, and inflammatory mediators, such as cytokines and chemokines, which further mediate tissue damage and coordinate the subsequent activation and function of both innate and adaptive immunity [9,33]. Therefore, neutrophils have previously been regarded as harmful cells in MI. However, recent studies have revealed that neutrophils also exhibit anti-inflammation properties and promote tissue repair during cardiovascular inflammation [5,8]. Macrophages in the ischemic myocardium are highly plastic and participate in the process of tissue damage and repair, which is manifested by a phenotypic transformation from pro-inflammation to anti-inflammation [2]. Evidence suggests that

Fig. 6. Ym-1 derived from neutrophils at the early stage of MIRI improves heart damage of MIRI mice. (a) Western blot and statistical analysis showing the expression of Ym-1 in immune cells at different time points of MIRI ($n = 3$ in each group). The expression of indicated proteins was normalized to that of Vinculin. (b) Flow cytometry and statistical analysis of the main source of Ym-1 1 d after reperfusion ($n = 6$). (c) Experimental design of the *in vivo* Ym-1 inhibition experiment. (d) Representative echocardiography of mice 1 d after reperfusion (LVIDd, left ventricular internal diameter at end-diastole; LVIDs, left ventricular internal diameter at end-systolic) and statistical analysis of EF, FS, LVEDV, and LVESV used to evaluate cardiac function ($n = 6$ in each group). (e) Statistical analysis of serum enzymology, including CK-MB, α -HBDB, AST, and LDH, in mice from each group 1 d after reperfusion ($n = 8$ in each group). (f) Representative Evans blue/TTC staining images of the heart and quantitative analysis of infarct size per cross-section of the left ventricle ($n = 5$ in each group). (g) Representative cardiac histopathologic images with HE staining in each group (scale bar = 100 μ m). (h) Experimental design of the *in vivo* Ym-1 supplementary experiment. (i) Representative echocardiography of mice 1 d after reperfusion and statistical analysis of EF, FS, LVEDV, and LVESV used to evaluate cardiac function ($n = 6$ in each group). (j) Statistical analysis of plasma enzymology in mice from each group 1 d after reperfusion ($n = 8$ in each group). (k) Representative Evans blue/TTC staining images of the heart and quantitative analysis of infarct size per cross-section of the left ventricle ($n = 5$ in each group). (l) Representative cardiac histopathologic images with HE staining in each group (scale bar = 100 μ m). Data are presented as the mean \pm SD. * $P < 0.05$, ** $P < 0.01$, *** $P < 0.001$. Each animal experiment was repeated independently at least three times.

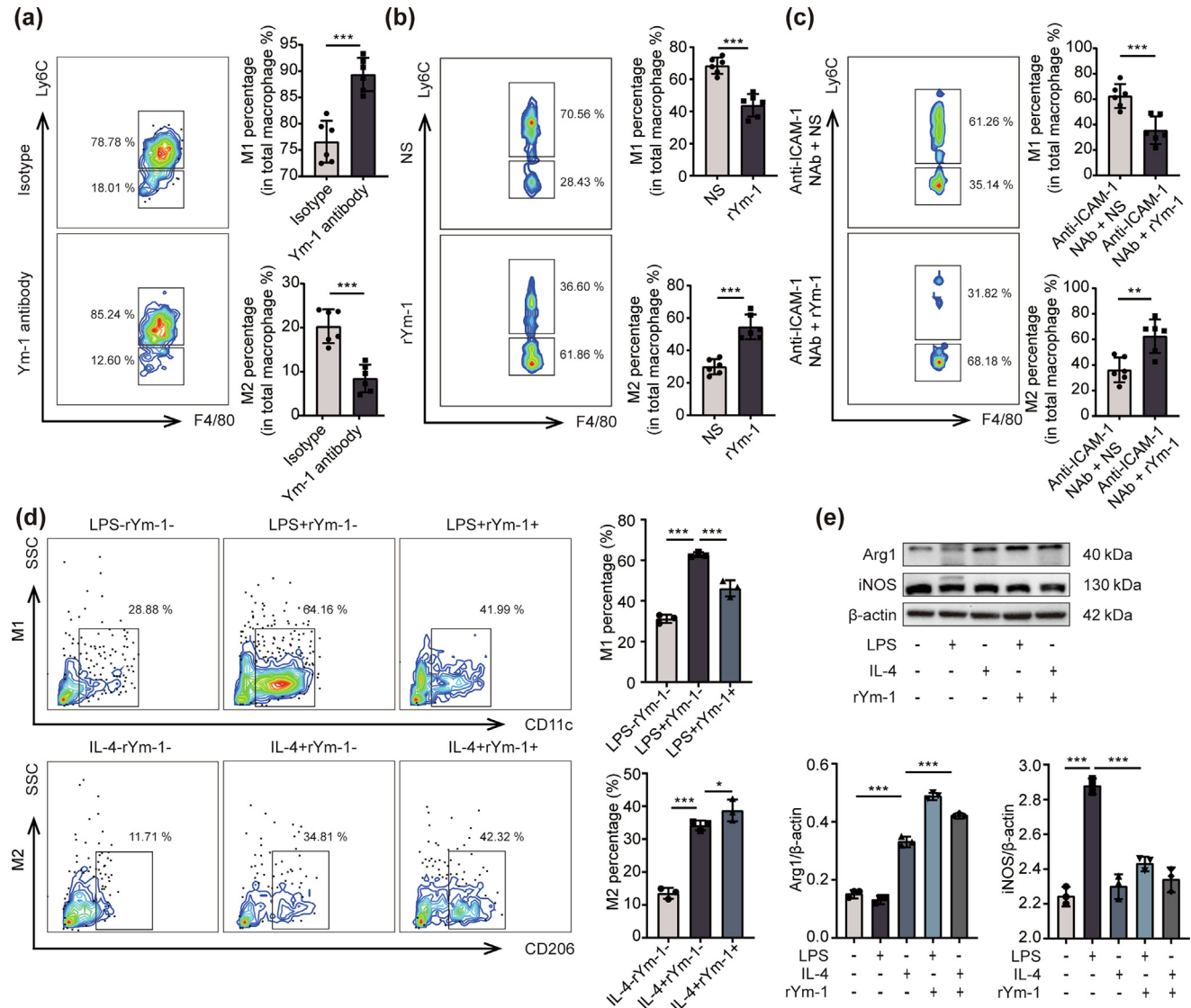


Fig. 7. Ym-1 exerts a cardioprotective role by driving macrophage polarization. Representative images of cardiac macrophage subsets detected by using flow cytometry and statistical analysis of the M1 and M2 expression 3 d after reperfusion in the experiments of (a) Ym-1 inhibition, (b) rYm-1 supplementation, and (c) anti-ICAM-1 + rYm-1 supplementation ($n = 6$ in each group). (d) Representative images and statistical analysis of induced polarization of bone marrow-derived macrophages (BMDM) *in vitro* with different interventions ($n = 3$ in each group). Upper panel shows LPS-induced M1; lower panel shows IL-4-induced M2. (e) Western blot and statistical analysis showing the expression of iNOS (marker for M1) and Arg1 (marker for M2) in LPS/IL-4-induced BMDM ($n = 3$ in each group). The expression of indicated proteins was normalized to that of β-actin. Data are presented as the mean \pm SD. * $P < 0.05$, ** $P < 0.01$, *** $P < 0.001$. Each animal experiment was repeated independently at least three times.

neutrophils play a crucial role in the transformation process by helping reprogram monocytes and macrophages [8]. Furthermore, according to the dichotomy of macrophages, neutrophils in infarcted hearts also present pro-inflammatory and anti-inflammatory subsets, suggesting that neutrophils are indeed heterogeneous in ischemic myocardial tissue.

Our scRNA-seq analysis showed that although macrophages were dominated in myocardial homeostasis and reperfusion injury, neutrophils were the first circulating cells responding and migrating to the diseased heart largely since reperfusion occurred, reaching a peak on day 1 and then rapidly returning to the baseline. Cluster analysis revealed that neutrophils in MIRI can be divided into five subsets featured by different functions according to their distinctive genes and time-specific expression. The dynamic expression of individual clusters is attributed to the multi-functions of neutrophils displayed at different time courses of MIRI progression. Among all neutrophils in MIRI, Ccl3^{hi} Neu was the dominant cell group at the early stage of reperfusion and was sub-

sequently replaced by Ym-1^{hi} Neu; the difference in the time-specific expression pattern of neutrophils after reperfusion was also attributed to the abundance of the two clusters.

Cardiac neutrophil subsets are assigned different functions in both MIRI and MI, but the response and peak reaction of the neutrophils in MIRI occur much earlier than those in MI [10,20], suggesting that the difference in immune responses between MI and MIRI cannot be attributed solely to the time window. Furthermore, the SiglecF^{hi} neutrophils, which specifically acquire this phenotype in the heart, show increased phagocytosis and reactive oxygen species production over time [5,34]. Although the exact function of SiglecF on the surface of the neutrophils remains unclear, evidence suggests that the SiglecF^{hi} subset may be a crucial cluster mediating tissue repair in MI [5]. We did not observe this group of myocardial neutrophils in the reperfusion hearts, indicating that the pathological mechanism of MIRI is different from that of MI. However, it also cannot be ruled out that the differences among cells are partly due to the different platforms used for scRNA-seq

analysis. Indeed, at 6 h after reperfusion, myocardial infiltrated neutrophils highly expressed chemokines and exhibited a high BM score, which is consistent with the phenomenon of rapid mobilization of BM-derived neutrophils to the damaged heart in response to stimulation during MI and early reperfusion [35,36]. As expected, we also detected peripheral neutrophils with high chemokine expression at 6 h after reperfusion of the heart. Notably, these cells also express specific molecules, including *Hif* and *Cebpb*, which may be responsible for their unique functions. One day after reperfusion, high-chemokine-expressing neutrophils declined sharply and were replaced by the subset featured by Ym-1-specific over-expression. Moreover, the cells highly expressed a variety of genes related to angiogenesis and tissue repair, similar to siglecF^{hi} neutrophils in MI, acquired related phenotypes in the heart. Therefore, we speculate that Ym-1^{hi} Neu may contribute to tissue repair in MIRI. Interestingly, the cardiac neutrophils decreased in the early stage of MIRI when different NAb were used to remove or inhibit neutrophil migration. However, the degree of myocardial injury varied owing to the heterogeneity of neutrophils that appeared upon treatment with NAb. For example, immunofluorescence data showed that the expression of Ym-1^{hi} Neu in the heart of mice treated with anti-ICAM-1 NAb was significantly lower than that in the hearts of mice treated with anti-Ly6G NAb, indicating that Ym-1^{hi} Neu is indeed involved in myocardial tissue repair. However, the mechanism by which anti-Ly6G NAb, but not anti-ICAM-1 NAb, affects the abundance of Ym-1^{hi} Neu in cardiac tissue remains unclear.

Ym-1, also known as Chi3l1 in human, is a class of proteins lacking chitinase activity and is an eosinophil chemotactic factor strongly induced by parasite infection [37]. Ym-1 is an innate immune regulatory factor widely present in prokaryotes and eukaryotes [38]. As a secreted protein, Ym-1 is expressed by a variety of cells, including hepatic parenchymal cells, macrophages, monocytes, endothelial cells, and neutrophils [31,39], and has previously been identified as a specific marker of M2 macrophages, promoting the anti-inflammatory function of M2 macrophages by enhancing IL-10 production [40]. Our data indicated that Ym-1 was one of the most differentially expressed proteins in neutrophils with an anti-inflammatory phenotype based on either cluster analysis or time-specific analysis, and neutrophils were the main source of Ym-1 in cardiac immune cells at the early stage of MIRI. We also found traces of Chi3l1^{hi} Neu in human atherosclerotic plaques, indicating the clinical potential of Chi3l1^{hi} Neu. In addition, Ym-1 is associated with a variety of chronic inflammatory diseases, including atherosclerosis [41,42] and obesity [43], and its plasma level has been correlated with the prognosis of patients with MI. However, its specific function remains to be elucidated. This finding suggests that neutrophils contribute to subsequent macrophage polarization in ischemic cardiomyopathy. Extensive associations between neutrophils and macrophages were also revealed by communication analysis in our study. Given the preferential expression of Ym-1 in macrophage subsets and the predominance of neutrophils in the early stage of reperfusion injury, we hypothesized that Ym-1^{hi} Neu, which is highly expressed after 1 d of reperfusion, might be involved in regulating macrophage polarization and may play a cardiac protective role by driving macrophages toward the repair phenotype. Experimentally, Ym-1 inhibition exacerbated cardiac damage, whereas the administration of Ym-1 recombinant protein led to limited myocardial injury in mice suffering from MIRI. The expression of anti-inflammatory macrophages in the cardiac tissue was significantly increased on day 3 of reperfusion. The same result was also observed in ICAM-1-treated model mice administered Ym-1 recombinant protein, suggesting that Ym-1 supplementation at the early stage of reperfusion compensated for the treatment failure caused by ICAM-1-induced loss of Ym-1^{hi} Neu in the cardiac tissue. During BMDM

differentiation *in vitro*, Ym-1 also promoted the expression of M2 macrophages but inhibited the M1 subset, which confirms its regulation of macrophage polarization again and indicates that targeting Ym-1^{hi} neutrophils in the early stage of MIRI is an effective strategy for improving MIRI.

In conclusion, our study demonstrates the dynamic characteristics of cardiac immune cells in MIRI and specifies the sentinel and dominant roles of neutrophils in the early stages of the disease. We also reveal the characteristics of neutrophils with heterogeneity and time-specific expression and identify a unique tissue-specific Ym-1^{hi} Neu subset featuring a repair phenotype, which is a crucial cluster determining tissue repair after reperfusion injury that exerts a cardioprotective effect by regulating macrophage polarization. Therefore, the modulation of Ym-1^{hi} neutrophils may represent a new strategy for the prevention and treatment of myocardial injury and repair in MIRI.

Conflict of interest

The authors declare that they have no conflict of interest.

Acknowledgments

This work was supported by the National Natural Science Foundation of China (82022076, 81974249, 82070136, 82104488, and 82305194), the Postdoctoral Science Foundation of China (2023M731222, and 2020T130040ZX), and the Foundation of Hubei Key Laboratory of Biological Targeted Therapy (2023swbx021).

Author contributions

Desheng Hu and Yalan Dong designed the study. Yalan Dong and Zhenyu Kang performed model establishment, single-cell isolation and library construction. Yalan Dong and Zili Zhang analyzed the data. Yalan Dong, Zhenyu Kang, Haifeng Zhou, Yanfei Liu, Xinxin Shuai, Liangqingqiang Yin, Xunxun Wang and Yan Ma performed the experiments detection. Yalan Dong, Shanshan Luo, Desheng Hu and Yue Liu wrote the manuscript. Yongqiang Zhang, Congzhu Ding, Junyi Li, Kim Yun Jin, Alexey Sarapultsev, Fangfei Li, Ge Zhang, Tian Xie, Changjun Yin, Xiang Cheng and Yue Liu revised the manuscript. Yue Liu, Desheng Hu, Shanshan Luo, Yalan Dong and Zhenyu Kang supervised the whole project. All authors have read and approved the article.

Data availability

The single-cell sequencing data of this study has been deposited in the Gene Sequence Archive (GSA) database of the National Genomics Data Center (NGDC, <https://ngdc.cncb.ac.cn/>). China National Center for Bioinformation / Beijing Institute of Genomics, Chinese Academy of Science (GSA: CRA012199). The other data supporting the findings of this study are available from the corresponding author on a reasonable request.

Appendix A. Supplementary materials

Supplementary materials to this article can be found online at <https://doi.org/10.1016/j.scib.2024.02.003>.

References

- [1] Sun K, Li YY, Jin J. A double-edged sword of immuno-microenvironment in cardiac homeostasis and injury repair. *Signal Transduct Tar* 2021;6:79.

- [2] Jin K, Gao S, Yang P, et al. Single-cell RNA sequencing reveals the temporal diversity and dynamics of cardiac immunity after myocardial infarction. *Small Methods* 2022;6:e2100752.
- [3] Ruiz-Villalba A, Romero JP, Hernandez SC, et al. Single-cell RNA sequencing analysis reveals a crucial role for CTHRC1 (Collagen Triple Helix Repeat Containing 1) cardiac fibroblasts after myocardial infarction. *Circulation* 2020;142:1831–47.
- [4] Kuppe C, Ramirez FR, Li Z, et al. Spatial multi-omic map of human myocardial infarction. *Nature* 2022;608:766–77.
- [5] Vafadarnejad E, Rizzo G, Krampert L, et al. Dynamics of cardiac neutrophil diversity in murine myocardial infarction. *Circ Res* 2020;127:e232–49.
- [6] Zlatanova I, Pinto C, Silvestre JS. Immune modulation of cardiac repair and regeneration: The art of mending broken hearts. *Front Cardiovasc Med* 2016;3:40.
- [7] Puhl SL, Steffens S. Neutrophils in post-myocardial infarction inflammation: Damage vs. Resolution? *Front Cardiovasc Med* 2019;6:25.
- [8] Horckmans M, Ring L, Duchene J, et al. Neutrophils orchestrate post-myocardial infarction healing by polarizing macrophages towards a reparative phenotype. *Eur Heart J* 2017;38:187–97.
- [9] Phillipson M, Kubes P. The healing power of neutrophils. *Trends Immunol* 2019;40:635–47.
- [10] Ma Y, Yabluchanskiy A, Iyer RP, et al. Temporal neutrophil polarization following myocardial infarction. *Cardiovasc Res* 2016;110:51–61.
- [11] Xia N, Lu Y, Gu M, et al. A unique population of regulatory T cells in heart potentiates cardiac protection from myocardial infarction. *Circulation* 2020;142:1956–73.
- [12] Xia M, Jiao L, Wang XH, et al. Single-cell RNA sequencing reveals a unique pericyte type associated with capillary dysfunction. *Theranostics* 2023;13:2515–30.
- [13] Li Z, Yang Q, Tang X, et al. Single-cell RNA-seq and chromatin accessibility profiling decipher the heterogeneity of mouse gammadelta T cells. *Sci Bull* 2022;67:408–26.
- [14] Zhang C, Hao H, Wang Y, et al. Intercellular mitochondrial component transfer triggers ischemic cardiac fibrosis. *Sci Bull* 2023;68:1784–99.
- [15] Dong YL, Duan XY, Liu YJ, et al. Autotaxin-lysophosphatidic acid axis blockade improves inflammation by regulating Th17 cell differentiation in DSS-induced chronic colitis mice. *Inflammation* 2019;42:1530–41.
- [16] Xie Z, Yu W, Ye G, et al. Single-cell RNA sequencing analysis of human bone-marrow-derived mesenchymal stem cells and functional subpopulation identification. *Exp Mol Med* 2022;54:483–92.
- [17] Li M, Guo W, Dong Y, et al. Elevated exhaustion levels of NK and CD8(+) T cells as indicators for progression and prognosis of COVID-19 disease. *Front Immunol* 2020;11:580237.
- [18] Zhao YJ, Yi WJ, Wan XJ, et al. Blockade of ICAM-1 improves the outcome of polymicrobial sepsis via modulating neutrophil migration and reversing immunosuppression. *Mediat Inflamm* 2014;2014:195290.
- [19] Zhang J, Liang R, Wang K, et al. Novel CaMKII-delta Inhibitor hesperadin exerts dual functions to ameliorate cardiac ischemia/reperfusion injury and inhibit tumor growth. *Circulation* 2022;145:1154–68.
- [20] Yan X, Anzai A, Katsumata Y, et al. Temporal dynamics of cardiac immune cell accumulation following acute myocardial infarction. *J Mol Cell Cardiol* 2013;62:24–35.
- [21] Xie X, Shi Q, Wu P, et al. Single-cell transcriptome profiling reveals neutrophil heterogeneity in homeostasis and infection. *Nat Immunol* 2020;21:1119–33.
- [22] Burman A, Garcia-Milian R, Wood M, et al. Acetaminophen Attenuates invasion and alters the expression of extracellular matrix enzymes and vascular factors in human first trimester trophoblast cells. *Placenta* 2021;104:146–60.
- [23] Sun Q, Yang Y, Wang Z, et al. PER1 interaction with GPX1 regulates metabolic homeostasis under oxidative stress. *Redox Biol* 2020;37:101694.
- [24] Ouyang J, Xiong Y, Shang H, et al. LAPTM5 Restricts HIV-1 infection in dendritic cells and is counteracted by Vpr. *Microbiol Spectr* 2022;10:e138221.
- [25] Kouzu H, Tatekoshi Y, Chang HC, et al. ZFP36L2 suppresses mTORC1 through a P53-dependent pathway to prevent peripartum cardiomyopathy in mice. *J Clin Invest* 2022;132.
- [26] Murase T, Yamamoto T, Koide A, et al. Temporal expression of chitinase-like 3 in wounded murine skin. *Int J Legal Med* 2017;131:1623–31.
- [27] Kong FQ, Zhao SJ, Sun P, et al. Macrophage MSR1 promotes the formation of foamy macrophage and neuronal apoptosis after spinal cord injury. *J Neuroinflammation* 2020;17:62.
- [28] Evrard M, Kwok I, Chong SZ, et al. Developmental analysis of bone marrow neutrophils reveals populations specialized in expansion, trafficking, and effector functions. *Immunity* 2018;48:364–79.
- [29] Kosti CN, Vaitsi PC, Pappas AG, et al. CSF1/CSF1R signaling mediates malignant pleural effusion formation. *JCI Insight* 2022;7.
- [30] Anversa P, Reiss K, Kajstura J, et al. Myocardial infarction and the myocyte IGF1 autocrine system. *Eur Heart J* 1995;16 Suppl N:37–45.
- [31] Sutherland TE, Ruckerl D, Logan N, et al. Ym1 induces RELMalpha and rescues IL-4Ralpha deficiency in lung repair during nematode infection. *PLoS Pathog* 2018;14:e1007423.
- [32] Murray PJ, Allen JE, Biswas SK, et al. Macrophage activation and polarization: Nomenclature and experimental guidelines. *Immunity* 2014;41:14–20.
- [33] Papayannopoulos V. Neutrophil extracellular traps in immunity and disease. *Nat Rev Immunol* 2018;18:134–47.
- [34] Calzago DM, Zhang C, Toomre A, et al. SiglecF(HI) marks late-stage neutrophils of the infarcted heart: A single-cell transcriptomic analysis of neutrophil diversification. *J Am Heart Assoc* 2021;10:e19019.
- [35] Petzold T, Zhang Z, Ballesteros I, et al. Neutrophil “plucking” on megakaryocytes drives platelet production and boosts cardiovascular disease. *Immunity* 2022;55:2285–99.
- [36] Fan Q, Tao R, Zhang H, et al. Dectin-1 contributes to myocardial ischemia/reperfusion injury by regulating macrophage polarization and neutrophil infiltration. *Circulation* 2019;139:663–78.
- [37] Di Rosa M, Tibullo D, Saccone S, et al. CHI3L1 nuclear localization in monocyte derived dendritic cells. *Immunobiology* 2016;221:347–56.
- [38] Raes G, De Baetselier P, Noel W, et al. Differential expression of FIZZ1 and Ym1 in alternatively versus classically activated macrophages. *J Leukoc Biol* 2002;71:597–602.
- [39] Starosom SC, Campo CJ, Woelfle T, et al. Chi3l3 induces oligodendrogenesis in an experimental model of autoimmune neuroinflammation. *Nat Commun* 2019;10:217.
- [40] Choi JW, Kwon MJ, Kim IH, et al. Pyropia yezoensis glycoprotein promotes the M1 to M2 macrophage phenotypic switch via the STAT3 and STAT6 transcription factors. *Int J Mol Med* 2016;38:666–74.
- [41] Yamamoto S, Zhong J, Yancey PG, et al. Atherosclerosis following renal injury is ameliorated by pioglitazone and losartan via macrophage phenotype. *Atherosclerosis* 2015;242:56–64.
- [42] Hayes EM, Tsaousi A, Di Gregoli K, et al. Classical and alternative activation and metalloproteinase expression occurs in foam cell macrophages in male and female ApoE null mice in the absence of T and B lymphocytes. *Front Immunol* 2014;5:537.
- [43] Shaul ME, Bennett G, Strissel KJ, et al. Dynamic, M2-like remodeling phenotypes of CD11c+ adipose tissue macrophages during high-fat diet-induced obesity in mice. *Diabetes* 2010;59:1171–81.



Yalan Dong received her Ph.D. degree from Huazhong University of Science and Technology in 2022. She is currently a postdoc at Union Hospital, Tongji Medical College, Huazhong University of Science and Technology. Her research focuses on the immune regulatory mechanism of cardiovascular diseases and the therapy of integrated traditional Chinese and Western medicine.



Zhenyu Kang received her Ph.D. degree from Wuhan Institute of Virology, Chinese Academy of Sciences. She is currently a postdoc at Union Hospital, Tongji Medical College, Huazhong University of Science and Technology. Her research focuses on the pathogenesis of cardiac ischemia-reperfusion and the pathogenesis of virulent pathogens.



Zili Zhang received his master's degree from Huazhong University of Science and Technology in 2023. He is interested in mechanisms of innate immunity and leverages single-cell sequencing to map the immune landscape in the tissue injury.



Yue Liu is currently a professor at Cardiovascular disease center, Xiyuan Hospital of China academy of Chinese medical sciences. He dedicates to the clinical transformation research on prevention and therapy of metabolic cardiovascular diseases by integrated traditional Chinese and Western medicine, and elucidates the modern mechanism of "Active Blood Circulation" in Chinese medicine by muti-technical means.



Shanshan Luo is currently a professor at Union Hospital, Tongji Medical College, Huazhong University of Science and Technology. Her research focuses on the regulation mechanism of innate immune system components in Hematological System and effective targets screening.



Desheng Hu is currently a professor at Union Hospital, Tongji Medical College, Huazhong University of Science and Technology. He is interested in the immune regulatory mechanism of tertiary lymphoid tissue in the microenvironment of cardiovascular diseases and screening new effective ingredients in Chinese medicine.